Paredes A, Justo-Méndez R, Jiménez-Blasco D, Núñez V, Calero I, Villalba-Orero M, Alegre-Martí A, Fischer T, Gradillas A, Sant'Anna VAR, Were F, Huang Z, Hernansanz-Agustín P, Contreras C, Martínez F, Camafeita E, Vázquez J, Ruiz-Cabello J, Area-Gómez E, Sánchez-Cabo F, Treuter E, Bolaños JP, Estébanez-Perpiñá E, Rupérez FJ, Barbas C, Enríquez JA, Ricote M. γ-Linolenic acid in maternal milk drives cardiac metabolic maturation. Nature. 2023 Jun;618(7964):365-373. doi: 10.1038/s41586-023-06068-7. Epub 2023 May 24. Erratum in: Nature. 2023 Jul;619(7968):E24. PMID: 37225978.

which has been published in final form at: https://doi.org/10.1038/s41586-023-06068-7

γ-linolenic acid in maternal milk drives cardiac metabolic maturation

Ana Paredes[1], Raquel Justo-Méndez[1], Daniel Jiménez-Blasco[2,3,4], Vanessa Núñez[1], Irene Calero[1], María Villalba-Orero[1,5], Andrea Alegre[6], Thierry Fischer[7], Ana Gradillas[8], Viviane Aparecida Rodrigues Sant'Anna[8], Felipe Were[9], Zhiqiang Huang[10], Pablo Hernansanz-Agustín[1], Carmen Contreras[1], Fernando Martínez[9,11], Emilio Camafeita[11,12], Jesús Vázquez[11,12], Jesús Ruiz-Cabello[13,14,15,16], Estela Area-Gómez[17,18], Fátima Sánchez-Cabo[9], Eckardt Treuter[10], Juan Pedro Bolaños[2,3,4], Eva Estébanez-Perpiñá[6], Francisco Javier Rupérez[7], Coral Barbas[7], José Antonio Enríquez[1,4], Mercedes Ricote[1,*]

[1]Cardiovascular Regeneration Program. Centro Nacional de Investigaciones Cardiovasculares (CNIC), Madrid, Spain.

[2]Institute of Functional Biology and Genomics (IBFG), University of Salamanca, CSIC, Salamanca, Spain.

[3]Institute for Biomedical Research of Salamanca (IBSAL), Salamanca, Spain.

[4]Centro de Investigaciones Biomédicas en Red en Fragilidad y Envejecimiento Saludable (CIBERFES), Madrid, Spain.

[5]Departamento de Medicina y Cirugía Animal, Universidad Complutense de Madrid (UCM), Madrid, Spain.

[6]Department of Biochemistry and Molecular Biomedicine, Institute of Biomedicine (IBUB) of the University of Barcelona (UB), Barcelona, Spain.

[7]Department of Immunology and Oncology, Centro Nacional de Biotecnología-Consejo Superior de Investigaciones Científicas (CNB/CSIC) Campus Universidad Autónoma de Madrid (UAM), Madrid, Spain.

[8]Centro de Metabolómica y Bioanálisis (CEMBIO), Facultad de Farmacia, Universidad San Pablo-CEU, CEU Universities, Madrid, Spain.

[9]Bioinformatics Unit, Centro Nacional de Investigaciones Cardiovasculares (CNIC), Madrid, Spain.

[10]Department of Biosciences and Nutrition, Karolinska Institutet, Huddinge, Sweden .

[11]Centro de Investigaciones Biomédicas en Red de Enfermedades Cardiovasculares (CIBERCV), Madrid, Spain.

[12]Proteomics Unit, Centro Nacional de Investigaciones Cardiovasculares (CNIC), Madrid, Spain.

[13]CIC biomaGUNE, Basque Research and Technology Alliance (BRTA), San Sebastian, Guipuzcoa, Spain.

[14]Ikerbasque, Basque Foundation for Science, Bilbao, Spain.

[15]Centro de Investigación Biomédica en Red - Enfermedades Respiratorias (CIBERES), Instituto de Salud Carlos III, Madrid, Spain.

[16]Departamento de Ciencias Farmacéuticas, Facultad de Farmacia, Universidad Complutense Madrid (UCM), Madrid, Spain.

[17]Departament of Cellular and Molecular Biology, Centro de Investigaciones Biológicas Margarita Salas-CSIC, Madrid, Spain.

[18]Department of Neurology, Columbia University Medical Campus, New York, USA.

*Correspondence: mricote@cnic.es (M.R.)

Summary

Birth presents a metabolic challenge to cardiomyocytes as they reshape fuel preference from glucose to fatty acids for postnatal energy production[1,2]. This adaptation is partly triggered by post-partum environmental changes[3], but the molecules orchestrating cardiomyocyte maturation

remain unknown. Here we show that this transition is coordinated by maternally supplied γ-linolenic acid (GLA), an 18:3 omega-6 fatty acid enriched in the maternal milk. GLA binds and activates retinoid X receptors (RXR)[4], ligand-regulated transcription factors expressed in cardiomyocytes from embryonic stages. Multifaceted genome-wide analysis revealed that the lack of RXR in embryonic cardiomyocytes caused an aberrant chromatin landscape that prevented the induction of an RXR-dependent gene expression signature controlling mitochondrial fatty acid homeostasis. The ensuing defective metabolic transition featured blunted mitochondrial lipid-derived energy production and enhanced glucose consumption, leading to perinatal cardiac dysfunction and death. Finally, GLA supplementation induced RXR-dependent expression of the mitochondrial fatty acid homeostasis signature in cardiomyocytes, both *in vitro* and *in vivo*. Thus, our study identifies the GLA-RXR axis as a key transcriptional regulatory mechanism underlying the maternal control of perinatal cardiac metabolism.

Main

The mammalian heart requires a continuous supply of energy to maintain cardiac contraction. The highly flexible metabolism of cardiomyocytes enables them to meet their ATP needs by consuming a broad spectrum of substrates, including glucose, lipids, lactate, amino acids, and ketone bodies, depending on physiological context and age[5]. Fetal cardiomyocytes primarily rely on glucose and lactate oxidation, but the main ATP source after birth is mitochondrial lipid oxidation[1,2,5,6]. However, while the importance of mitochondria in the adult heart is well-established, their contribution to fetal and perinatal heart function has been less explored. The cardiac fetal-to-neonatal switch is believed to occur progressively during the first two weeks of life, culminating in a functional mitochondrial compartment in which fatty acids are efficiently oxidized by β-oxidation (FAO)[7]. This adaptive step is crucial for the maintenance of heartbeat and survival, yet very little is known about the molecular mechanisms and upstream signals that instruct this metabolic transition.

Retinoid X receptors (RXR) are a nuclear receptor subfamily of ligand-regulated transcription factors that specifically respond to 9-*cis* retinoic acid and various endogenous fatty acids[8]. Since RXRs operate both as permissive homo- and heterodimers, their ability to be activated by dietary compounds defines them as molecular master sensors that transduce external cues into transcriptional programs[4]. RXR isoforms are encoded by 3 genes (mouse: *Rxra*/*Nr2b1*, *Rxrb*/*Nr2b2*, *Rxrg*/*Nr2b3)* which show time-specific and tissue-dependent differential expression. Whole-body knockout (KO) mice lacking RXRα show impaired myocardial growth and die between E13.5 and E16.5[9,10]. However, specific RXRα depletion in ventricular cardiomyocytes provokes no cardiac morphological defects, thus excluding a cell-autonomous role of cardiomyocyte-expressed RXRα[11]. We and others reported that RXR isoforms show redundancy in several contexts[9,12,13]; however, previous studies have not addressed RXR redundancy in the heart, and the physiological role of RXRs in cardiomyocyte homeostasis remains unknown.

RXR deletion causes lethal cardiac dysfunction

Analysis of RXR isoforms in embryonic and adult hearts revealed progressive increases in *Rxra* and *Rxrb* expression from developmental stages to adulthood, whereas *Rxrg* expression was restricted to postnatal cardiomyocytes (Extended data Fig.1a). To dissect RXR function in cardiomyocytes during development, we generated a RXR loss-of-function mouse model by crossing Nkx2.5Cre mice, which specifically targets the embryonic myocardium[14], with *Rxra* and *Rxrb* floxed mice (*Rxra*$^{f/f}$*b*$^{f/f}$)[12]. This approach allowed us to avoid compensatory effects between RXR isotypes during cardiac development.

The hearts of embryonic double-KO mice (Nkx2.5Cre$^{+/-}$*Rxra*$^{f/f}$*b*$^{f/f}$, hereafter edKO) efficiently deleted *Rxra* and *Rxrb* from E11.5 on (Extended data Fig.1b). Although edKO newborns were born at Mendelian frequency (data not shown), 80% of edKO pups died during the first 24 hours of life, and no edKO newborn survived beyond day 7 after birth (Fig.1a). Extensive echocardiography assessment revealed that edKO progressively underwent severe contractile dysfunction, as shown by gradually decreased ejection fraction (LVEF) within the first 24 hours (Fig.1b, Extended data Fig.1c, Supplemental video 1-2). This change was accompanied by pathological alterations in stroke volume (SV), cardiac output and LV end-systolic volume over time. Despite these alterations, left ventricle diastolic dimension did not change, presumably due to the rapid onset of the death (Extended data Fig.1c). The cardiac impairment preceded morbidity of the newborns, suggesting that these heart abnormalities likely contribute to neonatal death. In line with this, edKO hearts also showed increased expression of the cardiac stress markers *Anf* and *Bnp* (Fig.1c). These results demonstrate that cardiomyocyte-expressed RXRs exert a cell-autonomous function in the myocardium.

Remarkably, histological analysis of edKO hearts revealed no morphological myocardial abnormalities preceeding this cardiac malfunction (Extended data Fig.1d-f). Myocardial thickness and the ratio of non-compacted (NC) to compacted (C) myocardium were normal (Extended data Fig.1d). edKO pups were slightly smaller than controls but showed no evidence of cardiac hypertrophy (%HW/BW) or differences in cardiac diameter (Extended data Fig.1f-g).

Electrocardiogram (ECG) analysis of P0 newborns revealed typical ECG traces, with no differences from controls in QRS complex duration; or PR, QTc, and P intervals (Extended data Fig.1h), thus ruling out a contribution to the functional defects from altered rhythmic patterns. We also ruled out leaky expression of the Nkx2.5Cre driver in the brain, liver, stomach, thymus, diaphragm, and spleen (Extended data Fig.1i). Although subtle gene deletion was observed in the tongue, as previously reported[15], edKO displayed visible milk spots yet in a lesser extent that control pups (Extended data Fig.1j), probably due to a competing disadvantage against wild-type littermates. Further analysis excluded functional irregularities of the lungs (Extended data Fig.1k-m) or alternative systemic alterations such as thermogenesis (Extended data Fig.1n). These data thus reveal the existence of an unexplored physiological mechanism through which cardiomyocyte-expressed RXRs sustain cardiac function and neonatal survival.

RXRs drive switch to neonatal metabolism

Gene expression profiling of P0 hearts (Fig.1h-j) identified 145 significantly upregulated genes (adjusted p-value≤0.05, fold-change≥1.5) and 192 significantly downregulated genes (adjusted p-value≤0.05, fold-change≤-1.5) in the edKO model. Gene ontology analysis highlighted strong downregulation of essential lipid homeostasis-related processes, such as FAO, cholesterol biosynthesis, and the L-carnitine mitochondrial shuttle (Fig.1d). Dysregulated lipid metabolism was further evidenced by transcriptional dampening of the fatty acid-homeostasis signature in edKO hearts (Fig.1e). Notably, 26.05% of the downregulated genes (50 of 192) encode mitochondrial proteins related to lipid-derived energy production (Fig.1f). We called this gene subset the mitochondrial fatty acid homeostasis (mtFAH) cluster. RT-qPCR analysis of the mtFAH gene signature at gestational and perinatal stages revealed a sharp induction of mtFAH genes from E18.5 to P0 in control hearts. In contrast, mtFAH cluster expression was curtailed in edKO mice at P0, coinciding with the time death (Fig.1g). Prominent cardiomyocyte-intrinsic RXR-controlled genes detected in this analysis included critical components of lipid droplet homeostasis (*Plin5)*, fatty acid activation (*Acsl1* and *Acot1*), fatty acid import to the mitochondrial matrix (*Cpt1a, Cpt1b, Cpt2 and Slc25a20*), β-oxidation (*Acadvl, Hadha and Hadhb*), glucose/fatty acid catabolism balance (*Pdk4* and *Fbp2*), lipid-derived energy dissipation (*Ucp3*), ketogenesis (*Hmgcs2*), and lipogenesis (*Scd4* and *Dgat2*) (Extended data Fig.2a). This finding would appear to challenge the view that cardiomyocytes acquire the capacity for ATP generation from mitochondrial FAO progressively over the first 15 days of life[5] and suggests instead that cardiomyocytes require mitochondria equipped with the FAO machinery immediately after birth.

To investigate the mechanisms through which transcriptional dysregulation in the edKO heart might lead to defective lipid-derived energy generation in perinatal cardiomyocytes, we measured ATP production by cardiac P0 mitochondria fed with pyruvate (Pyruvate+Malate), glutamate (Glutamate+Malate), succinate, or and palmitate (Palmitate+Carnitine) (Fig.2a). No significant between-genotype differences in ATP production were detected when the substrate was pyruvate, glutamate, or succinate, indicating that entry to the electron transport chain by NADH (pyruvate and glutamate) and $FADH_2$ (succinate) was not significantly altered in edKO mitochondria. In contrast, ATP generation by β-oxidation from palmitate was significantly weakened in edKO mitochondria. Together with this result, edKO hearts significantly diminished the rate of palmitate oxidation (Fig.2b) and decreased fatty acid mitochondrial respiration (Fig.2c), overall indicating impaired fatty acid import or use. In agreement with these results, an unbiased lipidomics approach highlighted that depletion of RXRs resulted in significantly lower typical FAO metabolites such as long-chain acylcarnitines (C14 to C18)[16,17], and fatty acid esters of hydroxy fatty acids (FAHFAs) (Fig.2d, Supplementary Table 1).Remarkably, proteomics analysis of edKO hearts further confirmed that RXR deletion reduced the abundance of proteins involved in lipid handling (Fig.2e). Moreover, the hearts of edKO mice showed altered expression of several proteins related to mitochondrial dynamics and homeostatic pathways, such as ROS production, degradome, the mitochondrial unfolded protein response (mtUPR) (Extended data Fig.2b). These finding suggest that cardiomyocyte-specific RXR deletion results in the failure of cardiac mitochondrial remodeling toward lipid consumption and synthesis.

This effect was not linked to any alterations to the morphology (Extended data Fig.2c-d) or number (Extended data Fig.2e) of edKO mitochondria. Defective lipid-derived ATP production in the absence of RXR suggested that edKO hearts might commit their metabolism toward anaerobic glucose use. Significantly increased activity of both processes was confirmed by *ex vivo* quantification of glycolytic flux and lactate production (Fig.2f-g). In parallel, edKO mice displayed hypoglycemia and hyperlactaemia (Fig.2h-i), supporting the idea that RXRs are needed to initiate the fetal-to-neonatal transition, such that in their absence cardiomyocytes remain metabolically immature and unable to establish bioenergetic fitness.

GC/MS metabolomics profiling of the metabolic status of edKO hearts revealed a significant decrease in glycerol relative to controls, whereas uracil, creatinine, and aspartate were increased (Extended data Fig.2f). Uracil abundance correlated with the relative mRNA expression of *Upp1*, the uracil biosynthetic enzyme (Extended data Fig.2g). The generation of creatinine through the non-enzymatic cyclization of creatine is favored at low-pH[18], and the rise in creatinine could be due to a more acidic cellular environment resulting from the elevated lactate production in edKO hearts. In the case of aspartate, enhanced glucose oxidation is known to promote its biosynthesis in failing cardiomyocytes[19]. Aspartate is also intimately linked to α-ketoglutarate (α-KG), as both are end-products of glutamate and oxaloacetate transamination[20]. These findings prompted us to explore whether amino acids might contribute to energy homeostasis by replenishing Krebs cycle intermediates. While the amino acid oxidation rate was unaltered in edKO hearts (Extended data Fig.2h), α-ketoglutarate levels were higher in edKO hearts (Extended data Fig.2i), suggesting imbalanced Krebs cycle activity. These results suggest that cardiomyocyte-expressed RXRs are critical integrators of energy production and mitochondrial maturation immediately after birth.

RXR remodels cardiac transcription

To determine the molecular basis of the altered metabolic status in P0 edKO hearts, we conducted a multifaceted genome-wide characterization by assay for transposase-accessible chromatin regions using sequencing (ATAC-seq)[21] and by chromatin immunoprecipitation sequencing (ChIP-seq) for H3K27ac, a histone modification that marks active enhancers and promoters (Fig.3a). The combination of these techniques allowed us to delineate dynamic changes in chromatin openness and activation upon RXR depletion (Fig.3). ATAC-seq captured 326 differentially open chromatin regions (adj. *P* value<0.05, $\log_2$FC>0.6) and 629 closed regions (adj. *P* value <0.05, $\log_2$FC<-0.6) in edKO vs control P0 hearts, whereas H3K27ac ChIP-seq identified 42 differentially active peaks (adj. *P* value <0.05, $\log_2$FC>0.6) and 650 inactive peaks (adj. *P* value <0.05, $\log_2$FC<-0.6) (Fig.3b, Extended data Fig.3a). The relative loss of open and active genomic regions in edKO hearts suggests that loss of RXRs impacts on the epigenetic landscape of activated genes in perinatal cardiomyocytes. Moreover, annotation analysis identified similar distributions of ATAC-seq and H3K27ac ChIP-seq differential peaks (Fig.3c, Extended data Fig.3b), with closed and inactive peaks both predominantly annotated as introns (40.22% and 42.62%, respectively) or intergenic regions (36.72% and 31.08%). This suggests

that in perinatal cardiomyocytes RXRs might play an important role in the distal regulation of chromatin access and transcription via enhancers (Fig.3c). In line with this idea, transcription factor motif enrichment analysis of these peaks revealed that one of the most frequently found binding motifs was the conventional RXR homodimer response element with 1 nucleotide spacing (DR1), together with motifs for other cardiac-related transcription factors (MEF2 family and GATA4) (Fig.3d). DR-1 motifs are also bound by peroxisome proliferator-activated receptor (PPAR), suggesting them to be plausible heterodimeric partners for cardiac RXRs. In support of this, we found that RXRs and PPARα share the mtFAH gene expression signature in neonatal hearts (Extended data Fig.3c). Importantly, since the intersection of closed and inactive loci upon RXR depletion demarked the mtFAH signature (Fig.3e, Extended data Fig.3d), RXRs are specifically required for adaptive epigenetic changes within the regulatory regions of the fatty acid homeostasis gene cluster.

To determine whether the cardiac RXR cistrome included the mtFAH signature, we conducted RXR ChIP-seq experiments in control and edKO neonatal cardiomyocytes. Differential occupancy analysis detected 6896 loci that contained RXR peaks (10829 peaks, adj. *P* value <0.05, $log_2FC>0.6$), defininig its cistrome. Transcription factor enrichment analysis revealed highest enrichment of DR1 and DR4 elements, known motifs for diverse RXR dimers (Extended data Fig.3e). Notably, mtFAH signature genes were annotated to the 185 loci overlapping between RXR ChIP-seq, closed ATAC-seq peaks and inactive H3K27ac ChIP-seq peaks (Fig.3f, Fig.3g), marking the functional RXR-regulated enhancers and promoters amongst all RXR-occupied candidate regions (Extended data Fig. 3f). Also, gene ontology analysis of the overlapping RXR loci identified lipid homeostasis-related pathways as the most significantly enriched biological process (Fig.3h) and mitochondria-related compartments as the most enriched cellular compartment (Fig.3i), respectively. We conclude that RXRs directly operate at enhancers and promoters to activate transcription of the mtFAH signature genes and control their surrounding epigenetic landscape in perinatal cardiomyocytes.

Milk-FA drives cardiac RXR functions

To confirm that RXR activity directly controls the mtFAH signature and other lipid metabolism-related genes, we gavaged 8-week-old mice (C57Bl6/J) with the selective RXR agonist bexarotene[12]. RT-qPCR analysis of cardiac tissue showed that bexarotene significantly induced expression of the mtFAH and other lipid-metabolism genes (Extended data Fig.4a), validating the use of this synthetic ligand to modulate RXR-dependent transcriptional circuits in myocardial cells.

The identity of endogenous RXR ligands is a long-standing question given the central role of RXRs in controlling metabolic homeostasis across life span[22]. In newborns, maternal milk is a powerful source of signaling molecules able to trigger metabolic adaptions by increasing blood lipid content[3,7]. To investigate the impact of lactation on the RXR-dependent mtFAH signature, we analyzed relative mRNA expression in control and edKO hearts from maternal milk-fed or fasted P0 newborns (Extended data Fig.4b). *Rxra* and *Rxrb* transcripts were unaltered in fed and

fasted control hearts, indicating that maternal milk does not influence RXR abundance (Extended data Fig.4c). However, expression of mtFAH genes (*Slc25a20, Ucp3, Hmgcs2, Plin5, Pdk4*) and other lipid homeostasis genes (*Dgat2, Scd4*) was significantly reduced in fasted control mice, resembling the edKO transcriptional phenotype (Extended data Fig.4d). Maternal milk deprivation had no effect on lipid homeostasis gene expression in edKO hearts, suggesting that RXRs are important receptors for milk-derived inducers of the mtFAH transcriptional program.

Maternal milk is highly enriched in vitamin A and lipids[23,24], the metabolic precursors of RXR ligands[25]. Moreover, nutritional intervention in pregnant mice efficiently modulates maternal milk composition[26]. We therefore investigated whether a lack of fatty acids or vitamin A compounds in milk would prevent RXR-dependent mtFAH transcriptional induction in offspring (Fig.4a, Extended data Fig.4e-g). For these experiments, we crossed Nkx2.5Cre$^{+/-}$*Rxra*$^{f/+}$*b*$^{f/f}$ males with *Rxra*$^{f/f}$*b*$^{f/f}$ females, and *Rxra*$^{f/f}$*b*$^{f/f}$ dams were fed either a normal chow diet (NCD), a fat-free (FFD), or a vitamin A deficient (VAD) diet from E0.5 on. Lactation was monitored, and control and edKO hearts were collected from pups 4h after birth (Fig.4a). Hearts from neonates suckling VAD milk had a normal mtFAH gene expression profile, indicating that 9-cis retinoic acid is not the relevant RXR ligand in perinatal cardiomyocytes (Extended data Fig.4e). In contrast, hearts from pups suckling FFD milk showed a pronounced reduction in the expression of mtFAH signature genes and other lipid metabolism-related genes (Fig.4b), matching the effect observed in milk-deprived neonates (Extended data Fig.4d). Other key metabolic genes involved in glycolysis, Krebs cycle or mitochondrial oxidative phosphorylation complexes were not changed in FFD-milk feeding hearts (Extended data Fig.4f). The residual mtFAH signature in edKO hearts was largely insensitive to FFD–milk feeding, with only mild decreases in *Ucp3* and *Plin5* gene expression (Fig.4b). Because expression of *Rxra* and *Rxrb* was insensitive to FFD milk (Extended data Fig.4g), these data support the conclusion that cardiomyocyte-expressed RXRs relay signals from maternal milk-derived fatty acids (milk-FA) to allow mitochondrial maturation and metabolic adaptation in neonatal hearts.

To determine whether lack of milk-FA reproduces the RXR-deficient phenotype, we examined control newborns suckled with either NCD or FFD milk upon delivery. Whereas NCD milk-fed neonates thrived, FFD milk-fed control mice died within 48h of birth (Fig.4c) and showed a significant reduction in body weight at P1 (Extended data Fig.4h). Echocardiography analysis showed that FFD–milk suckling severely impaired cardiac function (Fig.4d, Extended data Fig.4i, Supplemental video 3-4). Cardiac defects in FFD milk-fed control mice included significantly decreased heart rate, stroke volume, cardiac output, and LVEF compared to NCD milk-fed pups (Fig.4d, Supplemental video 3-4). Moreover, the hearts of FFD milk-fed pups showed reduced LV telediastolic volume (Extended data Fig.4i). Consistent with these findings, FFD milk-fed neonates had significantly elevated cardiac expression of *Bnp* mRNA (Fig.4e). We excluded other possibilities of FFD demise, such as thermogenesis or lung edema (Extended data Fig.4j-k). In addition, FFD milk-fed control hearts blunted fatty acid mitochondrial respiration and enhaced glycolysis and lactate production (Fig.4f-g). Together, these results indicate that milk-FA supports

metabolic adaptation in the neonatal heart and suggest that activation of a milk-FA–RXR axis is a relevant mechanism for sustaining perinatal life.

GLA-RXR drives mitochondrial maturation

We next aimed to identify the endogenous RXR ligand in maternal milk. To precisely dissect the contribution of each milk-FA, we performed an unbiased lipidomics analysis comparing the fatty acid profiles of regular and fat-free milks (Supplementary Table 2). Milk-FAs that were significantly diminished in fat-free milk would be candidate RXR ligands. We detected 45 free fatty acids and estimated their abundance as the relative proportion within their fatty acid class: saturated (SAFA), monounsaturated (MUFA), di-unsaturated (DUFA) and polyunsaturated (PUFA). Interestingly, the family of omega-6 (ω-6) fatty acids showed the most significant reduction in milk from FFD-fed dams (*P* value<0.05, $\log_2$FC<0, mean content in NCD milk>0.5%). Specifically, linoleic acid (LA, C18:2n-6), γ-linolenic acid (GLA, C18:3n-6), dihomo-γ-linolenic acid (DGLA, C20:3n-6), and eicosadienoic acid (EDA, C20:2n-6) (Fig.4h, Extended data Fig.4l-m). ω-6 fatty acids are a family of important bioactive PUFAs generated through an elongation cascade from LA, an essential fatty acid that can be only provided by dietary intake and therefore cannot be compensated by endogenous maternal synthesis[27] (Fig.4i). The presence of LA, GLA, DGLA, and EDA has been widely reported in human breast milk, which thus provides the required physiological source of ω-6 fatty acids to the newborn[27-30].

LA and GLA bind the ligand-binding domain of RXRα and stabilize RXRα heterodimerization, respectively[31,32]. To assess whether these ω-6 fatty acids induce the mtFAH signature, we analyzed gene expression in C57B6/J primary neonatal cardiomyocytes and HL-1 cardiac muscle cell line treated with LA or GLA (Extended data Fig.5a-d). The synthetic RXR agonist LG268[12] was used as an additional pharmacological approach and served as a control. GLA and LG268 both strongly increased the abundance of mtFAH genes, whereas LA had no effect (Extended data Fig.5a-d). We further demonstrated that GLA-induced mtFAH gene expression is RXR-dependent, as the GLA effect was lost in edKO primary cardiomyocytes (Fig. 4j) as well as in C57B6/J primary neonatal cardiomyocytes pretreated with UVI3003 (UVI), an RXR antagonist[33] (Extended data Fig.5e). GLA absolute concentration (from all lipid forms) was further determined in cardiac tissue (30.4 µmol/kg) as well as in milk (NCD: 1066.3 µM ± 167.4 µM vs FFD; 335.9 µM ± 165.4 µM), which showed that FFD milk displayed a 3-fold decrease in total GLA.

Additionally, to validate the physiological role of maternal milk-derived GLA in metabolic cardiac maturation, we aimed to rescue the FFD phenotype by selectively restoring GLA levels in FFD milk (Fig. 4k). Newborns fed a FFD+GLA milk (GLA) thrived and restored body weight, glycemia and the ability to feed properly compared to FFD pups (Fig.4l, Extended data Fig.5f-h). Moreover, mtFAH gene expression in GLA perinatal hearts was significantly increased (Fig.4m, Extended data Fig.5i), postulating this maternal fatty acid as a critical signal to ensure neonatal cardiac transcriptional energetics. We also found that *in vivo* FFD+GLA recovery of survival is RXR-dependent, supporting the transcriptional axis GLA-RXR in perinatal cardiomyocytes

(Fig.4n). As alternative approaches, customized FFD diets supplemented with LA+GLA or GLA rescued FFD newborn lethality (Extended data Fig.5j). Notably, pups delivered by NCD mothers and exposed to FFD milk died, supporting that maternal milk, and not lipid deposits during pregnancy, is the relevant GLA source for ensuring perinatal survival (Fig.4o).

In order to provide more direct evidence that GLA binds to RXR, we first confirmed its interaction with the recombinant RXRα-LBD in vitro by surface plasmon resonance (SPR) (Fig.5a), showing that unliganded RXRα-LBD bound GLA with a (K_D) of 10.9 ± 7.1 μM. Moreover, GLA binding to the RXRα-LBD induced the recruitment of an SRC coactivator-derived LxxLL peptide with a (K_D) of 80.9 ± 3.6 μM (Fig.5b-c). This result indicates that, in the presence of RXR ligand, the AF2 coactivator-binding surface had acquired the active conformation capable of recruiting coactivators[34]. We further used a GAL4-UAS-driven luciferase reporter to monitor the activity of the wild-type RXRα(LBD)-GAL4(DBD) or RXRα(LBD)-ΔAF2-GAL4(DBD), expressing a mutant RXR that lacks the AF2 helix 12 required for ligand-dependent transcriptional activation[9,35], in the presence of GLA (Fig.5d). While GLA treatment significantly induced luciferase activity when wild-type RXRα was expressed, RXRα(LBD)-ΔAF2-GAL4(DBD)-expressing cells remained insensitive (Fig.5d). Remarkably, blockade of GAL4-RXRα binding by the RXR antagonist UVI3003 abolished GLA-mediated luciferase induction (Fig.5d). In addition, we corroborated the ability of GLA to stabilize RXRα/SRC1 coactivator complex in a ligand-dependent manner (Fig.5e). These assays were reproduced in an alternative system where RXRα or RXRα-ΔAF2 plasmids were cotransfected with a reporter plasmid containing 3 copies of the $(AOX)_3$ response element (RXRE-specific binding sites) (Extended data Fig.5k-m). Finally, *in silico* modeling revealed structural docking of GLA in the RXRα ligand-binding pocket, generating a stable GLA–RXRα complex (Fig.5f, Supplemental Table 3). Overall, these data demonstrate that GLA is a potential ligand for RXRs.

Discussion

The neonatal cardiac dysfunction and death of mice lacking cardiomyocyte RXRα and RXRβ demonstrates that myocardial-specific RXRs have a cell-autonomous role in cardiac physiology. Furthermore, given the absence of cardiac abnormalities in ventricle-restricted RXRα-deficient mice[11] and the full RXRβ-deficient mice[36], our results show that RXR isotypes compensate for the lack of each other in myocardial cells. In agreement with previous reports [37,38], we have excluded myocardial RXRs as transcriptional controllers of cardiac morphogenesis. In this setting, the structural abnormalities observed in the myocardium of full RXRα-deficient mice [10] may be due to the loss of epicardial-specific RXRα action, which has been proposed to regulate cardiomyocyte growth via WNT signaling in a paracrine fashion[39].

Although our study identifies RXRs as the key transcription factors controlling the fetal-to-neonatal metabolic transition, the extent to which this action relies on RXR homodimers or heterodimers with other nuclear receptors is currently difficult to estimate. Transcription factor motif analysis indicates that the DR1 motif is enriched at RXR target gene loci, including the mtFAH signature. Intriguingly, the DR1 motif is recognized by both RXR homodimers and

heterodimers with PPARs, which are expressed in embryonic cardiomyocytes. Indeed, we show that PPARα-deficient neonatal hearts also display a downregulated mtFAH gene signature. However, unlike RXRs, PPARα is not essential in the heart since PPARα KO mice have a milder phenotype that does not compromise neonatal survival[40]. This could be a consequence of functional redundancy among the PPAR isoforms[9,12,13]. Alternatively, the cooperation of RXR with other transcription factors/nuclear receptors could contribute to the lethality in edKO mice. Along with the edKO phenotype, the induction of the mtFAH signature with the here identified endogenous ligand GLA and with the RXR-selective agonist LG268 strongly supports the active role of RXRs, irrespective of the distinct RXR dimer states.

Our results identify the essential ω-6 PUFA GLA as a critical maternal-milk nutrient for proper cardiac adaptation and survival in murine newborns, demonstrating that GLA is a potential RXR ligand in perinatal cardiomyocytes. In terms of mammalian evolution, the obligate dietary intake of GLA could establish a Go/No-Go checkpoint in newborns, since only dams that are not nutritionally deprived will be able to provide their progeny with GLA and thus support proper nutritional health and growth. We also found that non-essential fatty acids are dispensable for cardiac mitochondrial maturation, in line with a report that offspring survival is unaffected by conditional deletion of the key lipogenic enzyme PERK[41]. The death of edKO neonates makes it difficult to dissect the functional implications of GLA–RXR signaling on postnatal cardiac physiology. An intriguing question for future research is whether the GLA–RXR axis plays a conserved role during the perinatal adaptation of other organs.

A technical limitation of our study was the inability to specifically quantify GLA absolute amount in the GLA-supplemented maternal milk, and therefore we cannot exclude the possibility of other metabolites to be involved in this context. On the other hand, the potential relevance of our findings in human physiology need to be further investigated. Remarkably, carnitine-acylcarnitine translocase deficiency (CACTD) is a human life-threatening metabolic disease that provokes heart failure and neonatal death. Interestingly, it is caused by mutations in the RXR-controlled gene, SLC25A20[42]. Therefore, it would be interesting to explore whether modulation of RXR transcriptional pathways may constitute an effective therapeutic approach. From a nutritional standpoint, low GLA abundance in human maternal milk has been linked to length growth deficit in newborns[43], suggesting a potential role of this fatty acid in human neonatal physiology. Our results reinforce the emerging concept that mother–infant interactions in early life are major drivers of organismal physiology and highglight the importance of maternal milk ingestion for mitochondrial maturation of perinatal hearts, a finding with major implications for cardiac health.

References

1 Itoi, T. & Lopaschuk, G. D. The contribution of glycolysis, glucose oxidation, lactate oxidation, and fatty acid oxidation to ATP production in isolated biventricular working hearts from 2-week-old rabbits. *Pediatric research* **34**, 735-741, doi:10.1203/00006450-199312000-00008 (1993).

2 Lopaschuk, G. D. & Spafford, M. A. Energy substrate utilization by isolated working hearts from newborn rabbits. *The American journal of physiology* **258**, H1274-1280, doi:10.1152/ajpheart.1990.258.5.H1274 (1990).

3 Girard, J., Ferré, P., Pégorier, J. P. & Duée, P. H. Adaptations of glucose and fatty acid metabolism during perinatal period and suckling-weaning transition. *Physiol Rev* **72**, 507-562, doi:10.1152/physrev.1992.72.2.507 (1992).
4 Rőszer, T., Menéndez-Gutiérrez, M. P., Cedenilla, M. & Ricote, M. Retinoid X receptors in macrophage biology. *Trends Endocrinol Metab* **24**, 460-468, doi:10.1016/j.tem.2013.04.004 (2013).
5 Lopaschuk, G. D., Ussher, J. R., Folmes, C. D., Jaswal, J. S. & Stanley, W. C. Myocardial fatty acid metabolism in health and disease. *Physiol Rev* **90**, 207-258, doi:10.1152/physrev.00015.2009 (2010).
6 Lopaschuk, G. D., Spafford, M. A. & Marsh, D. R. Glycolysis is predominant source of myocardial ATP production immediately after birth. *The American journal of physiology* **261**, H1698-1705, doi:10.1152/ajpheart.1991.261.6.H1698 (1991).
7 Piquereau, J. & Ventura-Clapier, R. Maturation of Cardiac Energy Metabolism During Perinatal Development. *Front Physiol* **9**, 959, doi:10.3389/fphys.2018.00959 (2018).
8 Krężel, W., Rühl, R. & de Lera, A. R. Alternative retinoid X receptor (RXR) ligands. *Molecular and cellular endocrinology* **491**, 110436, doi:10.1016/j.mce.2019.04.016 (2019).
9 Mascrez, B. *et al.* The RXRalpha ligand-dependent activation function 2 (AF-2) is important for mouse development. *Development (Cambridge, England)* **125**, 4691-4707 (1998).
10 Sucov, H. M. *et al.* RXR alpha mutant mice establish a genetic basis for vitamin A signaling in heart morphogenesis. *Genes & development* **8**, 1007-1018, doi:10.1101/gad.8.9.1007 (1994).
11 Chen, J., Kubalak, S. W. & Chien, K. R. Ventricular muscle-restricted targeting of the RXRalpha gene reveals a non-cell-autonomous requirement in cardiac chamber morphogenesis. *Development (Cambridge, England)* **125**, 1943-1949 (1998).
12 Menendez-Gutierrez, M. P. *et al.* Retinoid X receptors orchestrate osteoclast differentiation and postnatal bone remodeling. *The Journal of clinical investigation* **125**, 809-823, doi:10.1172/jci77186 (2015).
13 Ricote, M. *et al.* Normal hematopoiesis after conditional targeting of RXRalpha in murine hematopoietic stem/progenitor cells. *Journal of leukocyte biology* **80**, 850-861, doi:10.1189/jlb.0206097 (2006).
14 Stanley, E. G. *et al.* Efficient Cre-mediated deletion in cardiac progenitor cells conferred by a 3'UTR-ires-Cre allele of the homeobox gene Nkx2-5. *The International journal of developmental biology* **46**, 431-439 (2002).
15 Moses, K. A., DeMayo, F., Braun, R. M., Reecy, J. L. & Schwartz, R. J. Embryonic expression of an Nkx2-5/Cre gene using ROSA26 reporter mice. *Genesis* **31**, 176-180, doi:10.1002/gene.10022 (2001).
16 Schooneman, M. G., Vaz, F. M., Houten, S. M. & Soeters, M. R. Acylcarnitines: reflecting or inflicting insulin resistance? *Diabetes* **62**, 1-8, doi:10.2337/db12-0466 (2013).
17 Koves, T. R. *et al.* Mitochondrial overload and incomplete fatty acid oxidation contribute to skeletal muscle insulin resistance. *Cell Metab* **7**, 45-56, doi:10.1016/j.cmet.2007.10.013 (2008).
18 Wyss, M. & Kaddurah-Daouk, R. Creatine and creatinine metabolism. *Physiol Rev* **80**, 1107-1213, doi:10.1152/physrev.2000.80.3.1107 (2000).
19 Ritterhoff, J. *et al.* Metabolic Remodeling Promotes Cardiac Hypertrophy by Directing Glucose to Aspartate Biosynthesis. *Circ Res* **126**, 182-196, doi:10.1161/circresaha.119.315483 (2020).
20 Zdzisińska, B., Żurek, A. & Kandefer-Szerszeń, M. Alpha-Ketoglutarate as a Molecule with Pleiotropic Activity: Well-Known and Novel Possibilities of Therapeutic Use. *Arch Immunol Ther Exp (Warsz)* **65**, 21-36, doi:10.1007/s00005-016-0406-x (2017).
21 Buenrostro, J. D., Wu, B., Chang, H. Y. & Greenleaf, W. J. ATAC-seq: A Method for Assaying Chromatin Accessibility Genome-Wide. *Curr Protoc Mol Biol* **109**, 21.29.21-21.29.29, doi:10.1002/0471142727.mb2129s109 (2015).
22 Szanto, A. *et al.* Retinoid X receptors: X-ploring their (patho)physiological functions. *Cell Death Differ* **11 Suppl 2**, S126-143, doi:10.1038/sj.cdd.4401533 (2004).
23 Silverman, J., Stone, D. W. & Powers, J. D. The lipid composition of milk from mice fed high or low fat diets. *Lab Anim* **26**, 127-131, doi:10.1258/002367792780745832 (1992).

24 J, Y. d. V., Pundir, S., McKenzie, E., Keijer, J. & Kussmann, M. Maternal Circulating Vitamin Status and Colostrum Vitamin Composition in Healthy Lactating Women-A Systematic Approach. *Nutrients* **10**, doi:10.3390/nu10060687 (2018).
25 Dawson, M. I. & Xia, Z. The retinoid X receptors and their ligands. *Biochimica et biophysica acta* **1821**, 21-56, doi:10.1016/j.bbalip.2011.09.014 (2012).
26 Oosting, A., Verkade, H. J., Kegler, D., van de Heijning, B. J. & van der Beek, E. M. Rapid and selective manipulation of milk fatty acid composition in mice through the maternal diet during lactation. *J Nutr Sci* **4**, e19, doi:10.1017/jns.2015.13 (2015).
27 Sergeant, S., Rahbar, E. & Chilton, F. H. Gamma-linolenic acid, Dihommo-gamma linolenic, Eicosanoids and Inflammatory Processes. *Eur J Pharmacol* **785**, 77-86, doi:10.1016/j.ejphar.2016.04.020 (2016).
28 Wright, S. & Bolton, C. Breast milk fatty acids in mothers of children with atopic eczema. *British Journal of Nutrition* **62**, 693-697, doi:10.1079/BJN19890069 (1989).
29 Vaidya, H. & Cheema, S. K. Breastmilk with a high omega-6 to omega-3 fatty acid ratio induced cellular events similar to insulin resistance and obesity in 3T3-L1 adipocytes. *Pediatr Obes* **13**, 285-291, doi:10.1111/ijpo.12215 (2018).
30 Okolska, G., Ziemlański, S., Kowalska, M. & Ostojska, J. The levels of essential unsaturated fatty acids in human milk on the 3rd, 4th, 5th, and 6th days after labour. *Acta Physiol Pol* **34**, 239-248 (1983).
31 Lengqvist, J. *et al.* Polyunsaturated fatty acids including docosahexaenoic and arachidonic acid bind to the retinoid X receptor alpha ligand-binding domain. *Mol Cell Proteomics* **3**, 692-703, doi:10.1074/mcp.M400003-MCP200 (2004).
32 Forman, B. M., Chen, J. & Evans, R. M. Hypolipidemic drugs, polyunsaturated fatty acids, and eicosanoids are ligands for peroxisome proliferator-activated receptors alpha and delta. *Proceedings of the National Academy of Sciences of the United States of America* **94**, 4312-4317, doi:10.1073/pnas.94.9.4312 (1997).
33 Watanabe, M. & Kakuta, H. Retinoid X Receptor Antagonists. *Int J Mol Sci* **19**, doi:10.3390/ijms19082354 (2018).
34 Henttu, P. M., Kalkhoven, E. & Parker, M. G. AF-2 activity and recruitment of steroid receptor coactivator 1 to the estrogen receptor depend on a lysine residue conserved in nuclear receptors. *Mol Cell Biol* **17**, 1832-1839, doi:10.1128/mcb.17.4.1832 (1997).
35 Niu, H. *et al.* Endogenous retinoid X receptor ligands in mouse hematopoietic cells. *Sci Signal* **10**, doi:10.1126/scisignal.aan1011 (2017).

Figure 1. edKO mice undergo lethal cardiac dysfunction and transcriptional alteration of lipid metabolism. (a) Kaplan-Meier curves for edKO and control mice (n=27-32 mice per genotype). Log-Rank test (P<0.0001). **(b)** Echocardiographic acquisition of edKO (n=6-9 mice/time) and control (n=5-11 mice/stage) mice (16-h and 21-h after birth). Left ventricle ejection fraction (LVEF%), Stroke Volume (µL), cardiac output (mL/min), and LV end-systolic volume (µL). Data as means±s.e.m. Two-way ANOVA (Tukey post-test). **(c)** RT-qPCR quantification of *Bnp* and *Anf* genes in P0 edKO (n=5-6 mice) and control (n=5-6 mice) hearts. Independent biological replicates. Data as means±s.e.m. Two-tailed Student t test. **(d)** IPA biological processes altered in P0 edKO hearts. Bar shading represents $-\log_{10}(P \text{ value})$. Red and blue bars indicate up- and downregulated terms, respectively. **(e)** Heatmap of normalized RNA-seq expression data for the top DEGs (n=3-4 mice per genotype, independent biological replicates). Genes are clustered according biological processes, with genes encoding mitochondrial proteins shaded red. **(f)** Chord diagram representing cellular component analysis of DEGs (downregulated) mitochondrial-protein-encoding genes in edKO P0 hearts. Shading of squares adjacent to gene symbols indicates the $\log_2$FC (edKO vs control). **(g)** Relative RT-qPCR quantification of FAO genes in developmental (E12.5, E14.5 and E18.5) and perinatal stages (P0) from edKO (n=3-6) and Control (n=4-6) hearts. Data were presented as means±s.e.m. Two-way ANOVA. Independent

biological replicates. *P<0.05, **P <0.01, ***P <0.001, ****P <0.0001, ns, not significant. Exact P values are provided in Source Data.

Figure 2. Lack of RXRs in perinatal cardiomyocytes blocks fetal-to-neonatal metabolic switch. **(a)** *Ex-vivo* ATP production assay in control (n=8-19) and edKO (n=4-18) P0 cardiac mitochondria supplied with Pyruvate+Malate, Glutamate+Malate, Succinate, or Palmitate+Carnitine. Individual biological replicates. Data as means±s.e.m. Two-tailed Student t test. **(b)** Ex-vivo β-oxidation flux in control (n=17) and edKO (n=18) P0 hearts. Individual biological replicates. Data as means±s.e.m. Two-tailed Student t test. **(c)** *Ex-vivo* oxygen consumption assay in control (n=5) and edKO (n=5-6) P0 cardiac mitochondria supplied with octanoyl-carnitine (fatty acid oxidation), Glutamate+Malate, succinate and the combination of all substrates. Individual biological replicates. Data as means±s.e.m. Two-tailed Student t test. **(d)** Unbiased lipidomics analysis in control (n=4) and edKO (n=4) P0 hearts. Acyl-carnitines (CAR) and fatty acid and fatty acid esters of hydroxyl fatty acid (FA, FAHFA) are depicted. Data presented as Fold-change (edKO vs Control). Independent biological replicates. Two-tailed Student t test. **(e)** Protein function enrichment plot of edKO (n=5) vs Control (n=5) P0 hearts. Independent biological replicates. Dot size indicates number of proteins in each term. The X-axis indicates the Zc value (edKO vs control), and the Y-axis indicates the $-\log_{10}$(FDRc value) (edKO vs control). **(f-g)** *Ex* vivo glycolytic flux (f) and lactate generation (g) (nmol x h^{-1}per mg tissue) in control (n=7) and edKO (n=7) P0 hearts. Independent biological replicates. Data as means±s.e.m. Two-tailed Student t test. **(h)** Blood glucose in control (n=48) and edKO (n=30) (P0) newborns. Individual biological replicates. Data as means±s.e.m. Mann Whitney test. **(i)** Blood lactate in control (n=16) and edKO (n=20) (P0) newborns. Individual biological replicates. Data as means±s.e.m. Mann Whitney test. *P<0.05, **P <0.01, ***P <0.001, ****P <0.0001, ns, not significant. Exact P values are provided in Source Data.

Figure 3. RXRs transactivate the expression of mtFAH genes. (a) Genome-wide analysis outline. **(b)** Left, H3K27ac ChIP-seq heatmap illustrating differentially active/inactive peaks in edKO hearts. Right, ATAC-seq heatmap showing differentially open/closed peaks in edKO hearts. Adj.P value<0.05, $\log_2$FC=0.6, (n=2-3 per genotype/experiment, independent biological replicates) **(c)** Annotation distribution of differentially closed peaks (ATAC-seq) and differentially inactive peaks (H3K27ac ChIP-seq) in edKO P0 hearts. **(d)** HOMER motif enrichment analysis in edKO P0 hearts. Top-scoring motifs, P values, best-match transcription factors, type of nuclear receptor binding DR element, and % of target and background sequences are shown. **(e)** Intersection of RNA-seq, H3K27ac ChIP-seq, and ATAC-seq experiments. For peaks found in only one experiment, a value of 0 was specified for the other axis. Blue and red dots indicate genes significantly downregulated or upregulated according to the $\log_2$FC (RNA-seq). Size indicates $-\log_{10}$(adjusted P value) (RNA-seq). Two-tailed Student t test (Benjamini-Hochberg). For loci absent in the RNA-seq experiment, a size of 1 was specified. **(f)** Venn diagram of the RXR cistrome (RXR ChIP-seq), differentially closed annotated *loci* (Closed ATAC-seq), and differentially inactive annotated *loci* (Inactive H3K27ac ChIP-seq) in edKO hearts. Numbers indicate the number of *loci* that contained annotated peaks in each experiment. The overlapping

section (185 *loci*) contains the mtFAH signature. **(g)** mtFAH *loci* UCSC tracks identified in the RXR ChIP-seq (n=2 hearts/genotype, independent biological replicates), H3K27ac ChIP-seq, and ATAC-seq experiments. Black, Control. Red, edKO. Scales are indicated for all *loci* and tracks. Genes encoding mitochondrial proteins are in red type. **(h-i)** GO enrichment of the 185 annotated mtFAH *loci* for biological process (h) and cellular component (i) analysis. X-axis represents fold-enrichment, dots are colored according to –log10(adj *P* value), and size is proportional to the gene ratio. Two-tailed Student t test (Benjamini-Hochberg post-test). FC, fold-change (edKO vs control). Mito, mitochondria. TG, triglycerides.

Figure 4. Maternal-borne GLA activates RXR-dependent gene signature. (a) Experimental outline. **(b)** Cardiac expression of mtFAH signature from control (n=10-17, solid) and edKO (n=11-14, dashed) mice (P0) suckled with regular (NCD) or fat-free-diet milk (FFD). Data as means±s.e.m. Two-way ANOVA (Tukey's). **(c)** Kaplan-Meier curve of NCD (n=58) or FFD (n=33) control mice. Log-Rank test (*P*<0.0001). **(d)** Echocardiography analysis from control newborns (P1) suckling NCD (n=4) or FFD (n=6) milk. Cardiac output as L/min. Data as means±s.e.m. Two-tailed Student t-test. **(e)** Cardiac *Bnp* expression from NCD-fed (n=10) or FFD-fed (n=17) newborns (P1). Data as means±s.e.m. Two-tailed Student t-test. **(f)** β-oxidation oxygen consumption assay in NCD (n=5) and FFD (n=5) cardiac mitochondria (P1). Data as means±s.e.m. Two-tailed Student t-test. **(g)** Glycolytic flux (left) and lactate generation (right) (nmol x h^{-1}/mg) in NCD (n=17) and FFD (n=17) P1 hearts. Data as means±s.e.m. Two-tailed Student t-test. **(h)** Relative abundance of ω-6 FA in NCD (n=6) and FFD (n=4) milk: linoleic acid (LA), γ-linolenic acid (GLA), dihomo-γ-linolenic acid (DGLA), and eicosadienoic acid (EDA). Data as means±s.e.m. Two-tailed Student t-test. **(i)** The ω-6 FA biosynthesis pathway. **(j)** *In vitro* mtFAH gene signature expression in control or edKO cardiomyocytes treated with GLA-BSA (500 µM). Data as means±s.e.m. (n=3 replicates/condition). Two-way ANOVA. **(k)** Outline for rescuing FFD neonatal phenotype. **(l)** Kaplan-Meier curve of control FFD-fed (n=64) or GLA+fat-free-diet-fed (GLA, n=18) milk. Log-Rank test (*P*=0.0003). **(m)** Cardiac mtFAH gene expression from NCD-fed (n=6), FFD-fed (n=8) or GLA-fed (n=21) mice. Data as means±s.e.m. One-way ANOVA (Tukey&Benjamini-Hochberg). **(n)** Kaplan-Meier curve of FFD-fed and GLA-fed control and edKO mice. Log-Rank test (n=8-20 mice/condition) (*P*=0.0002). **(o)** Kaplan-Meier curve of control newborns born from NCD mothers but exposed to NCD or FFD milk. Log-Rank test (*P*<0.0001) (n=15-22 mice/group). **P*<0.05, ***P*<0.01, ****P*<0.001, *****P*<0.0001. Independent biological samples in Fig.4b-h,l-o. Exact *P* values in Source Data.

Figure 5. γ–Linolenic acid is a potential ligand for RXRs. Surface plasmon resonance (SPR) analysis of unliganded RXRα-LBD interaction with increasing concentrations of GLA **(a)**, SRC2-3 coactivator **(b)**, and SRC2-3 coactivator in the presence of a saturating concentration of 120 µM GLA **(c)**. The results of experiments conducted in duplicate are shown along with the calculated affinity constants (KD). The 1:1 Langmuir fitting presented a Rmax (RU) and a Chi^2 (RU^2) of **(a)** 19.82 and 0.510, **(c)** 30.00 and 1.66, respectively. **(d)** Representative experiment (out of 3) of GAL4-UAS-driven luciferase reporter assay in HEK293.T cells. Cells transfected with empty

vector, wild-type RXRα(LBD)-GAL4(DBD) or mutated RXRα(LBD)-ΔAF2-GAL4(DBD) during 6 hours (n=3 technical replicates/condition). Then, cells were treated with GLA-BSA conjugated (500 µM) or GLA-BSA conjugated (500 µM) + RXR antagonist UVI3003 (UVI, 1 µM) during 24h. Data as means±s.e.m. Two-way ANOVA (Tukey post-test). **(e)** Representative experiment (out of 3) of GAL4-UAS-driven luciferase reporter assay to monitor ligand-dependent coactivator recruitment in HEK293.Tcells. Transient transfections performed with a limiting amount wild-type RXRα(LBD)-GAL4(DBD) and/or SRC1 coactivator during 6 hours. Then, cells were treated with GLA-BSA conjugated (500 µM) during 24h (n=3 technical replicates/condition). Data as means±s.e.m. Two-way ANOVA (Tukey post-test). **(f)** *In silico* model of GLA docking in the ligand-binding domain of the mouse RXRa dimer. Left, 3D view (cartoon representation) illustrating the RXRa chain A in green and chain B in cyan. The ligand cavity is represented as gray dots. Right, zoomed view of GLA docking in the ligand cavity of chain A. The ligand cavity is represented as gray dots and GLA as a yellow stick model. DBD, DNA binding domain; LBD, ligand-binding domain. **P*<0.05, ***P* <0.01, ****P* <0.001, *****P* <0.0001. Exact *P* values are provided in Source Data.

Methods

Mice. All experiments were performed according to local ethical guidelines and were approved by the Animal Subjects Committee of the Instituto de Salud Carlos III (Madrid, Spain) in accordance with EU Directive 86/609/EEC and Madrid Community Organs in the PROEX 188/26. All animals used in this study were generated on C57BL/6J background. Mice were housed at 2-5 animals per cage with a 12 hour light/dark cycle (lights on from 07:00 to 19:00h hrs) at constant temperature (23ºC) with *ad libitum* access to food and water, and 45%-65% of relative humidity. Mice were fed a normal chow diet (LASQCdiet Rod18-A), fat-free diet (TD.03314-160, Ssniff), vitamin A deficient diet (TD.86143, Ssniff), fat-free diet + 3% safflower oil + 3% borage oil (GLA+LA, TD.03314-162, Ssniff) and fat-free diet + 6% borage oil (GLA, TD.03314-163, Ssniff). In order to conditionally ablate *Rxra* and *Rxrb* in the developing heart, we crossed Nkx2.5Cre$^{+/-}$ heterozygous males[14] with females bearing *Rxra*$^{f/f}$[13] and *Rxrb*$^{f/f}$ [44] alleles. We finally obtained embryonic double RXR-KO mice: Nkx2.5Cre$^{+/-}$*Rxra*$^{f/f}$*b*$^{f/f}$ (edKO) after an additional crossing of heterozygous offspring Nkx2.5Cre$^{+/-}$*Rxrab*$^{f/+}$ with *Rxrab*$^{f/f}$ females. *Rxra*$^{f/f}$*b*$^{f/f}$ littermates were used as controls. PPARα-null mice were kindly provided by Dra. Guadalupe Sabio (CNIC). Genotyping was performed by PCR of genomic DNA extracted from tail snips. Total DNA was obtained using REDExtract-N-Amp Tissue PCR Kit (#R4775, Sigma). PCR conditions and primers are described in Supplementary Table 4. Male and female mice were studied during the whole study. In studies using P0 mice, pregnant females were monitorized according to vaginal plug. Before tissue collection, neonates were euthanized by decapitation. Adult animals were killed either by cervical dislocation or carbon dioxide (CO_2) asphyxiation. For in vitro experiments samples were allocated randomly in each experiment. Randomization was produced by blindly collecting tissues prior genotyping. In vivo experiments were reproduced 2-3 independent times.

Echocardiography analysis. Transthoracic echocardiography was performed on P0 newborns. Neonatal mice were not anesthetized. Mice were placed in a biofeedback warming station that control core body temperature. Warm ultrasound gel was applied to the chest of the animals, and echocardiography measurements were obtained using the VEVO 2100 high frequency ultrasound system with a linear transducer MS400 18-38 MHz (Visual Sonics, Toronto, Canada). Parasternal short- and long-axis views at 3 levels (base, middle and apex) in two-dimensional and M-mode were obtained as described previously[45]. The LV end-systolic and end-diastolic volume (LV Vol;s and LV Vol;d, respectively) were acquired from the parasternal two-dimensional short-axis view, and LV ejection fraction (LV EF) was calculated using the area-length method[46]. Wall thickness at the end of the systole and diastole was measured from the M-mode short-axis. Analysis was performed off-line by two blinded echocardiography experts. Ultrasounds were performed in collaboration with Dr. María Villlalba-Orero at CNIC.

Body temperature quantification. Whole body temperature of P0 newborns was quantified by thermographic images using a FLIR T430sc Infrared Camera (FLIR Systems, Inc., Wilsonville, OR) and analyzed through FlirIR software.

Wet/dry lung ratio. Lung tissue (P0 newborns) was weighted right after collection (wet) and then, after dessecation (dry) at 95ºC O/N. The ratio was calculated by dividing wet weight/dry weight of each corresponding sample.

Blood glucose and lactate determination. After decapitation, blood drops were collected and glucose and lactate levels were measured by a glucose tester (Hoffmann-La Roche, Basel, Switzerland) and lactate tester (Accutrend Plus, Roche diagnostics), respectively.

Effects of fasting and nutritional milk intervention on cardiac gene expression. In fasting experiments, 2 mg progesterone (Sigma, #P0130) were i.p. injected to pregnant females at E17.5 and E18.5. At E19.5, pregnant dams were euthanized by cervical dislocation and C-sections were performed. After 4 hours, neonates were euthanized by decapitation and hearts were collected. For milk intervention experiments, pregnant dams were fed a normal chow, fat-free or vitamin A-deficient diet from E0.5 on. After natural delivery, pups were allowed to suckle for 4 hours and then newborns were euthanized and hearts collected.

***In vivo* GLA supplementation.** Dams were fed a fat-free diet (TD.03314, Ssniff) from E0.5 and then gavaged with GLA (4 mg/kg, L2378 Sigma) daily from E12.5 on.

Bexarotene. 8 week-old C57BL6/J mice were treated with one dose of 10 mg/kg of bexarotene (200499, Sigma) by oral gavage. Five days after the treatment, mice were euthanized and hearts were collected for gene expression analysis.

Lipidomic profiling of milk samples by UHPLC-ESI-QTOF-MS analysis. For maternal milk extraction at day 1 post-partum, dams were i.p. treated with 4UI Oxytocin (Sigma, O325) and separated from their pups during 4h. Then, 50 µl of milk per female was obtained by manual stimulation.

1000 ppm solutions of the internal standards (IS) deuterated palmitic acid-d31 and C17 sphinganine (Merck/Sigma-Aldrich, Burlington MA, USA) were prepared in methanol, and diluted in a MMC solvent mixture, i.e. methanol, methyl tert-butyl ether and chloroform: MeOH/MTBE/CHCl3 4:3:3 v/v/v (all MS-grade from Honeywell, Charlotte NC, USA), so the final concentration of both IS was 15 ppm. Then, 10 µL of each milk sample were mixed in 0.5 mL microtubes with 70 µL of MMC including the IS, vortex-mixed for 20 min and centrifuged (10,800 g) at RT for 5 min. Finally, the supernatant was transferred to a chromatographic vial with insert, and 1 µL was injected onto the LC-MS system (approximately equivalent to 10 nL of milk).

Lipidomics data from milk samples were acquired using an Agilent 1290 Infinity II Ultrahigh Performance Liquid Chromatography (UHPLC) system coupled to an Agilent 6545 quadrupole time-of-flight (QTOF) mass spectrometer. The Agilent 1290 Infinity II Multisampler system, equipped with a multiwash option, was used to uptake 1 µL of extracted samples. The multisampler temperature was maintained at 15°C to preserve compounds in a stable environment and avoid lipid precipitation. An Agilent InfinityLab Poroshell 120 EC-C18 (3.0 × 100 mm, 2.7 µm) (Agilent Technologies) column and a compatible guard column (Agilent InfinityLab Poroshell 120 EC-C18, 3.0 × 5 mm, 2.7 µm) were used and maintained at 50°C. The chromatography gradient started at 70% of B at 0 – 1 min, 86% of B at 3.5 – 10 min, 100% of B at 11-17 min. The starting conditions were recovered by minute 17, followed by a 2 min re-equilibration time; the total running time was 19 min. The mobile phases used for both positive and negative ionization modes consisted of (A) 10 mM ammonium acetate, 0.2 mM ammonium fluoride in water/methanol (9:1, v/v) and (B) 10 mM ammonium acetate, 0.2 mM ammonium fluoride in acetonitrile/methanol/isopropanol (2:3:5, v/v/v). The flow rate was held constant, set at 0.6 mL/min. The multiwash strategy consisted of a mixture of methanol:isopropanol (50:50, v/v) with the wash time set at 15 s, and aqueous phase:organic phase (30:70, v/v) mixture to assist in the starting conditions.

The Agilent 6545 QTOF mass spectrometer equipped with a dual AJS Electrospray (ESI) ion source was set with the following parameters: 150 V fragmentor, 65 V skimmer, 3,500 V (Pos), 3,000 V (Neg) capillary voltage, 750 V octopole radio frequency voltage, 10 L/min nebulizer gas flow, 200°C gas temperature, 50 psi nebulizer gas pressure, 12 L/min sheath gas flow, and 300°C sheath gas temperature. Data were collected in positive and negative ESI modes in separate runs, operated in full scan mode from 50 to 1800 m/z with a scan rate of 3 spectra/s. A solution consisting of two reference mass compounds were used throughout the whole analysis: purine ($C_5H_4N_4$) at m/z 121.0509 for the positive and m/z 119.0363 for the negative ionization modes; and HP-0921 ($C_{18}H_{18}O_6N_3P_3F_{24}$) at m/z 922.0098 for the positive and m/z 980.0163 (HP-0921 + acetate) for the negative ionization modes. These masses were continuously infused into the system through an Agilent 1260 Iso Pump at a 1 mL/min (split ratio 1:100) to provide a constant mass correction. For both ionization modes, 10 Iterative-MS/MS runs were performed. They were operated with an MS and MS/MS scan rates of 3 spectra/s, 40-1800 m/z mass window, a narrow (~ 1.3 amu) MS/MS isolation width, 3 precursors per cycle, and a MS/MS threshold of 5,000 counts and 0.001%. Five iterative-MS/MS runs were set with a collision energy of 20 eV, and the

next five runs were performed at 40 eV. References masses and contaminants detected in blank samples were excluded from the analysis to avoid their inclusion in the iterative-MS/MS.

Workflow for lipid identification. All the iterative MS/MS spectra datasets collected after the LC-MS analyses, from data-dependent acquisition (DDA) in positive and negative ionization modes, were used for lipid molecular species identification using a strategy relied on two independent software tools: Agilent MassHunter LipidAnnotator™ [47](Agilent Technologies Inc., Santa Clara, CA, USA), and the open source software MS-DIAL 4[48] (RIKEN Center for Integrative Medical Sciences, Yokohama, Japan) to ensure high-confidence accurate lipid identification.

The annotation process was carried out in four steps: 1) The raw iterative-MS/MS data obtained was imported to both software to build a fragmentation-based (MS/MS) library comprising the *m/z* of all the precursors identified as lipids by the software, together with their corresponding retention time (RT). The method parameters were set as follows: Lipid Annotator™ vendor software: ion species $[M+H]^+$, $[M+Na]^+$, and $[M+NH_4]^+$ for positive; and $[M-H]^-$, and $[M+CH_3COOH-H]^-$ for negative ionization mode. Then, for both ion modes, the Q-Score was set at ≥ 50; all the lipid classes were selected, mass deviation was established as ≤ 20 ppm, fragment score threshold was fixed as ≥ 30, and total score was set at ≥ 60. MS-DIAL 4 open-source software. MS1 centroid data, MS/MS centroid data, positive ion mode, lipidomics as a target omics, MS1 tolerance and MS2 tolerance set at 0.01 Da and 0.025 Da, respectively. Retention time from 0 to 23 min, minimum peak height 1.000; mass slice width, 0.1 Da; smoothing level 3 scans, minimum peak width 5 scans and sigma window value, 0.5. Results from the two software were merged and filtered in an Excel file following the inclusion criteria: candidate matches at least in two software, within $\Delta RT < 0.3$ min; in the case that the compound is found just by one tool and the other tool does not yield any compound for that molecular feature, the total score is going to be a crucial point, it is higher than 80% is considered annotated and if it is not, a manual inspection of the MS/MS spectrum using MassHunter Qualitative 10.0 must be done; or candidate with the highest spectral matching. 2) The principal aim of this step is to remove false positives from the putative list obtained previously. Here, a manual MS/MS spectral interpretation was carried out using Agilent MassHunter Qualitative Analysis software (B.10.00). Specific fragments ions helped to resolve interferences on isobaric and isomeric peaks as well as the information available in databases such as Lipid Maps (www.lipidmaps.org). Then, an additional manual MS1 inspection is done to complete the series of fatty acid chain composition based on literature, retention time behaviors of each molecule backbone (chromatographic retention time (RT) mapping: mass-to-charge ratio (*m/z*) versus RT) and using our on-line tool CEU Mass Mediator (www.ceumass.eps.uspceu.es). At the end of this step, an in-house library containing molecular formulas, isotopic mass and retention times is generated. 3)Then, the in-house library is used to perform data mining by the Batch Targeted Feature Extraction (TFE) algorithm of Agilent MassHunter Profinder software (B.10.00). Finally, all peak area values of every molecular feature extracted was exported to an Excel file for a comparison of the major lipid classes and their fatty acid composition present in the fat-free versus regular milk samples. Changes observed (Supplemental file 2) are expressed as a fold change and percentage of change.

Absolute quantification of GLA in milk and hearts.

NCD milk (n=6 biological replicates), FFD milk (n=5 biological replicates) and control hearts (n=4 biological replicates) were used for the determination of total GLA by GC-FID following the methodology described[49]. Briefly, lipids were extracted in chloroform:methanol (2:1), and the extracts were evaporated to dryness under vacuum, resuspended in toluene and subjected to methanolysis for 2.5 h at 80°C in methanol:toluene (4:1) containing acetyl chloride. The FAME (fatty acid methyl esters) were separated and quantified on a Perkin Elmer gas chromatograph (Autosystem; Norwalk, CT, USA), with a flame ionisation detector and a 30 m × 0.25 mm Omegawax (Sigma) capillary column. Nitrogen was used as carrier gas. Purified standards of FAME were analysed for the calculation of the amount of GLA based on the comparison of the peak areas.

Lipidomic profiling of heart samples by UHPLC-ESI-QTOF-MS analysis.

Mice hearts were transferred to a sealed microtube and weighed. Then, 350 µL of Methanol:Water 1:1 v/v and 2 beads (stainless steel, 2 mm) were added. All samples were shaken at 50 Hz in a QIAGEN TissuLyser LT (Hilden, Germany) for 60 min, and then centrifuged at 15000 g for 5 min. 350 µL of Chloroform:Methanol 6:1 were added and the tubes were vortex-mixed (VXHDAL Ohaus, Nänikon Switzerland) 60 min at maximum speed. The tubes were centrifuged at 400 g for 10 min at room temperature. 100 µL of the lower phase were taken with a glass syringe and transferred to a vial with glass insert, and the solvent evaporated to dryness in a Gyrozen HyperVac VC2124 (Gimpo, Korea) coupled to a LVS 110Z (Gardner Denver Thomas GmbH Welch Vacuum, Fürstenfeldbruck, Germany). Samples were resuspended in 100 µL Methanol and directly transferred to the UHPLC system.

Lipidomics data from heart samples were acquired using an Agilent 1290 Infinity II Ultrahigh Performance Liquid Chromatography (UHPLC) system coupled to an Agilent 6545 quadrupole time-of-flight (QTOF) mass spectrometer. The Agilent 1290 Infinity II Multisampler system, equipped with a multiwash option, was used to uptake 1 µL of extracted samples. The multisampler temperature was maintained at 15°C to preserve compounds in a stable environment and avoid lipid precipitation. An Agilent InfinityLab Poroshell 120 EC-C18 (3.0 × 100 mm, 2.7 µm) (Agilent Technologies) column and a compatible guard column (Agilent InfinityLab Poroshell 120 EC-C18, 3.0 × 5 mm, 2.7 µm) were used and maintained at 50°C. The chromatography gradient started at 70% of B at 0 – 1 min, 86% of B at 3.5 – 10 min, 100% of B at 11-17 min. The starting conditions were recovered by minute 17, followed by a 2 min re-equilibration time; the total running time was 19 min. The mobile phases used for both positive and negative ionization modes consisted of (A) 10 mM ammonium acetate, 0.2 mM ammonium fluoride in water/methanol (9:1, v/v) and (B) 10 mM ammonium acetate, 0.2 mM ammonium fluoride in acetonitrile/methanol/isopropanol (2:3:5, v/v/v). The flow rate was held constant, set at 0.6 mL/min. The multiwash strategy consisted of a mixture of methanol:isopropanol (50:50, v/v) with the wash time set at 15 s, and aqueous phase:organic phase (30:70, v/v) mixture to assist in the starting conditions.

The Agilent 6545 QTOF mass spectrometer equipped with a dual AJS Electrospray (ESI) ion source was set with the following parameters: 150 V fragmentor, 65 V skimmer, 3,500 V (Pos), 3,000 V (Neg) capillary voltage, 750 V octopole radio frequency voltage, 10 L/min nebulizer gas flow, 200°C gas temperature, 50 psi nebulizer gas pressure, 12 L/min sheath gas flow, and 300°C sheath gas temperature. Data were collected in positive and negative ESI modes in separate runs, operated in full scan mode from 50 to 1800 m/z with a scan rate of 3 spectra/s. A solution consisting of two reference mass compounds were used throughout the whole analysis: purine (C5H4N4) at m/z 121.0509 for the positive and m/z 119.0363 for the negative ionization modes; and HP-0921 (C18H18O6N3P3F24) at m/z 922.0098 for the positive and m/z 980.0163 (HP-0921 + acetate) for the negative ionization modes. These masses were continuously infused into the system through an Agilent 1260 Iso Pump at a 1 mL/min (split ratio 1:100) to provide a constant mass correction. For both ionization modes, 10 Iterative-MS/MS runs were performed. They were operated with an MS and MS/MS scan rates of 3 spectra/s, 40-1800 m/z mass window, a narrow (~ 1.3 amu) MS/MS isolation width, 3 precursors per cycle, and a MS/MS threshold of 5,000 counts and 0.001%. Five iterative-MS/MS runs were set with a collision energy of 20 eV, and the next five runs were performed at 40 eV. References masses and contaminants detected in blank samples were excluded from the analysis to avoid their inclusion in the iterative-MS/MS.

All the iterative MS/MS spectra datasets collected after the LC-MS analyses, from data-dependent acquisition (DDA) in positive and negative ionization modes, were used for lipid molecular species identification using a strategy relied on Agilent MassHunter LipidAnnotator™ (Agilent Technologies Inc., Santa Clara, CA, USA).

The raw iterative-MS/MS data obtained was imported to the LipidAnnotator to build a fragmentation-based (MS/MS) library comprising the m/z of all the precursors identified as lipids by the software, together with their corresponding retention time (RT). The method parameters were set as follows: ion species [M+H]+, [M+Na]+, and [M+NH4]+ for positive; and [M-H]-, and [M+CH3COOH-H]- for negative ionization mode. Then, for both ion modes, the Q-Score was set at ≥ 50; all the lipid classes were selected, mass deviation was established as ≤ 20 ppm, fragment score threshold was fixed as ≥ 30, and total score was set at ≥ 60.

Cell culture and omega-6 fatty acid treatments. Neonatal CMs were isolated from P1-P3 C57Bl/6J, Control or edKO pups and cultured as previously described[50,51]. HL-1 cell line was cultured in Claycomb medium (51800C, Sigma) supplemented with 1%P/S, 2mM Gln and 10%FBS. Dishes were pre-coated with 1mg/ml Human Fibronectin (F2006, Sigma). For omega-6 fatty acid supplementation, 500.000 cells were seeded in p24 plates and treated with: 500 µM BSA-conjugated linoleic acid (LA, L9530 Sigma), 500 µM BSA-conjugated g-linolenic acid (GLA, L2378 Sigma) or 1µM LG268 (SML0279, Sigma) for 6 hours. For RXR antagonists assays, neonatal CMs were pretreated for 2 hours with 0.5 µM UVI3003 (3303, Tocris). Then, GLA-BSA conjugated 500 µM was added for 6 hours and RT-qPCR gene expression analysis was performed. For dose-response assays, GLA was serially diluted and neonatal CMs were treated for 6 hours which was followed by RT-qPCR gene expression analysis.

ECG and data analysis. P0 mice were acquired. Four-lead surface ECGs were recorded, for a period of 5 minutes, from subcutaneous 23-gauge needle electrodes attached to each limb using the MP36R amplificator unit (BIOPAC Systems). During offline analysis, lead II was used for QRS duration using AcqKnowledge 4.1 analysis software. A representative 30s segment of the recording was averaged to obtain the signal-averaged ECG. Then, ECG intervals duration was measured as the time interval between the earliest moment of deviation from baseline and the moment when the S-wave returned to the isoelectric line.

Histology. E18.5 embryonic hearts were extracted, washed twice in cold phosphate-buffered saline (PBS 1X) and fixed in 4% paraformaldehyde (#50-980-487, Fisher Scientific) overnight (O/N). After alcohol dehydration, tissues were embedded in paraffin and cut using a semi-automatic microtome. Transverse or longitudinal sections (7 µm) were with hematoxylin-eosin (H&E) according to standard procedures. Whole slide images were digitalized with a digital slide scanner (Hamamatsu, Nanozoomer-RS C110730) and visualized and exported to TIFF images using NDP.view2 software (Hamamatsu Photonics). For quantification, Fiji Imaje J Software (NIH, https://imagej.nih.gov/ij/) was used.

Quantitative real time PCR (RT-qPCR). Total RNA from neonatal tissues was isolated using Trizol (#T9424, Sigma-Aldrich) and MaXtract High Density tubes (#129056, Qiagen) followed by standard chloroform-isopropanol extraction. For neonatal hearts/spleen/thymus/diaphragm, RNA carrier (#1068337, Qiagen) was added according to manufacturer´s information. RNA was measured using a Nanodrop UV Visible Spectrophotomer (ThermoFisher Scientific) and cDNA was prepared with High-Capacity cDNA Reverse Transcription Kit (#4374966, ThermoFisher Scientific). Transcripts were quantified with SYBR™ Green PCR Master Mix (#4309155, Applied biosystems) using the system AB7900-FAST-384 with the following programme: 95ºC 15 min, (95ºC 10 seg, 60ºC 20 seg, 72ºC 30 seg) x 40 cycles, 95ºC 15 seg, 60ºC 15 seg, 95ºC 15 seg. Gene expression values were normalized to housekeeping genes *36b4* and *Cyclophilin*. For mRNA relative expression experiments, values were expressed as relative mRNA levels or fold changes compared to littermate controls. Data were analysed using qBASE (Biogazelle). For absolute expression quantification, Ct values were extrapolated into standard curves for *Rxra*, *Rxrb*, *Rxrg* and *Cyclophilin*. Primer sequences are listed in Supplemental Table 4.

Transmission electron microscopy. For transmission electron microscopy (TEM) images, the whole neonatal heart was processed. Tissues were fixed O/N 4ºC in 1ml of Karnovsky´s solution (5%Glutaraldehyde [#G5882, Sigma], 4% paraformaldehyde [#50-980-487, Fisher Scientific], 0.1M Cacodylate buffer [#C4945, Sigma] and 0.5mg/ml $CaCl_2$) followed by 3 PBS 1X washes. Samples were post-fixed using 1% Osmium tetroxide (in distilled water) for 1h at RT, washed twice with distilled water and stained with 0.5% uranyl acetate for 10 min (in distilled water). Samples dehydration consisted of ascending alcohol solutions (30%, 50%, 70%, 95% and 100%) and acetone. For embedding step, samples were included in Durcupan resin at incubated for 48 h at 60ºC. Ultra-thin sections (60 nm) were obtained with a Leica Ultracut S Ultramicrotome (Leica), placed in copper grids (200 mesh) and contrasted with uranyl acetate and lead citrate.

Images were acquired with Jeol Jem1010 de 100Kv (Tokyo-Japan) electron microscope coupled with Gatan Orius SC200 (Pleasanton CA) digital camera. For quantification, Fiji Imaje J Software (NIH, https://imagej.nih.gov/ij/) was used. Adobe Photoshop CC 19.1.5 and Adobe Illustrator CC v22.1 were used for downstream image analysis and illustration.

mtDNA and nDNA quantification. Copy number of mitochondrial DNA measurement was performed as described[52]. Briefly, genomic DNA was extracted from neonatal hearts using phenol:chloroform:isoamyl alcohol standard protocol. Nuclear DNA (nDNA) and mitochondrial DNA (mtDNA) were quantifying by qPCR *Hk2* and *Nd1* transcripts levels, respectively. Primer sequences are provided in Supplemental Table 4. Each neonatal heart was considered as individual biological replicates. mtDNA/nDNA quantification was calculated as follows:

$$\Delta\mathrm{Ct} = \mathrm{Ct}(\mathrm{nDNA\ gene}) - \mathrm{Ct}(\mathrm{mtDNA\ gene})$$

$$\frac{mtDNA}{nDNA} copy\ number = 2x2^{\Delta Ct}$$

ATP synthesis assay. Each neonatal heart was processed separately and considered as individual biological samples. Cardiac mitochondria were isolated as described previously[53]. Briefly, hearts were removed and immediately cooled at 4ºC in medium A (320mM sucrose, 10mM Tris-HCl, 1mM EDTA pH 7.4) with 1mg/ml fatty acid-free BSA (#A8806, Sigma). Tissue homogenization was performed with a glass tissue grinder using a motor-driven Teflon pestle (Heidolph RZR 2041) with 10-15 strokes at 600rpm followed by a centrifugation at 1000g for 5 min at 4ºC. Supernatant was sequentially centrifuged at 10000g for 5 min at 4ºC to spin down mitochondrial fraction. Mitochondria-containing pellets were resuspended in medium A and quantified using Bradford´s method[54]. ATP synthesis was performed as described previously[55]. Briefly, 25-50ug of mitochondrial protein were resuspended in buffer A (150mM KCl, 25mM Tris-HCl, 2mM EDTA, 0.1%fatty acid-free BSA, 10mM KPO_4, 0.1mM $MgCl_2$ pH 7.4) at RT and dispensed into the wells of a 96-well luminescence reading plate (Costar). Substrate cocktail and buffer B (0.5M Tris-acetate pH 7.75, 0.4mM luciferine [#E1601, Promega], 10ug/ml luciferase [from *Photinus pyralis,* #10411523001, Roche]) were added and luminescence was measured over 2 minutes in a plate luminometer (Orion Microplate Luminometer, Simplicity 4.2). Substrate cocktails were composed of 6mM of diadenosin pentaphospate (#D4022, Sigma) and 6mM ADP (#A2754, Sigma) supplemented with 0.1M glutamate/malate (G+M) [#G1626 and #M9138, Sigma], 0.1M pyruvate/malate (Pyr+M) [#P5280, Sigma], 0.1M succinate (Succ) [#398055, Sigma], 0.1M palmitate/L-Carnitine (FA) [#P9716, Sigma] or pyruvate/malate palmitate/L-carnitine (Pyr+FA). An ATP standard curve (0-10mM final concentration of ATP) and the consequent regression curve was performed to correlate ATP concentration and luminescence in cardiac samples. ATP production rate was expressed as nmol ATP/(min x mg protein) normalized vs control.

Oxygen consumption. 0.02mg/ml of cardiac mitochondria or tissue homogenate were resuspended in 2 ml of mir05 medium (https://www.bioblast.at/index.php/MiPNet22.10_MiR05-

Kit) and analysed using a Clark-type electrode (Oxygraph O2k; Oroboros Instruments). In order to permeabilize the cells. Fatty acids oxidation was measured with 0.2mM Octanoylcarnitine (Sigma 50892), 2.5mM ADP (Sigma 09015) and 0.1mM Malate (Sigma M1000). Next, CI-dependent oxygen consumption was measured by adding 10 mM glutamate (Sigma G1626) and 0.4 mM malate. Finally, CII-dependent oxygen consumption was measured by adding 10 mM succinate (Sigma S 2378). 2.5 µM antimycin A (Sigma A 8674) and 0.5 µM Rotenone (sigma R 8875) were added in order to discard the non-mitochondrial respiration for all the above-mention calculations. For normalization purpose, CIV-dependent oxygen consumption was measured with 0.5 mM TMPD and 2 mM ascorbate were added as well as 100mM azide after stabilization.

Determination of the beta-oxidation flux *ex vivo*. The beta-oxidation flux was measured by assessing the rate of conversion of [9,10-^{3}H(N)] palmitic acid into ^3H_2O. In essence, heart slices (5-10 mg) were pre-incubated for 30 min in 2 ml of a Krebs–Henseleit buffer (11 mM Na_2HPO_4, 122 mM NaCl, 3.1 mM KCl, 0.4 mM KH_2PO_4, 1.2 mM $MgSO_4$, 1.3 mM $CaCl_2$; pH 7.4, supplemented with 30 µM BSA-conjugated palmitic acid and 0.5 mg/ml BSA fatty acid free at 37 ºC, followed by incubation in the presence of 1 µCi/ml of [9,10-^{3}H (N)] palmitic acid in fresh Krebs-Henseleit buffer (2 ml) in glass 25-ml Erlenmeyer flasks equipped with a central well containing a tube with 0.5 ml of water. The flask atmosphere was gassed with a O_2/CO_2 (95/5) mixture for 20 s and stopped with a rubber cap, and the flasks were incubated in a thermostatized orbital shaker (Forma Benchtop Orbital Shaker, Model 420, Thermo Fischer) for 3 hours at 37°C. In preliminary experiments (data not shown), we observed that ^3H_2O collected in the tube placed in the central well was linear with time at least up to 4 hours. Incubations were finished by injecting 0.2 ml of 20 % (v/v) $HClO_4$ (Merck Millipore) through the rubber cap, and flasks were further incubated for 72 h to allow the equilibration of ^3H_2O between the incubation medium and the water of the central well. The rate of beta-oxidation was expressed as nmol of [9,10-^{3}H] palmitic acid converted into ^3H_2O per hour and per mg of heart.

Glycolytic flux. The glycolytic flux was measured by assessing the rate of conversion of D-[3-^{3}H] glucose into ^3H_2O, as previously described[56]. In essence, heart slices (5-10 mg) were pre-incubated for 30 min in 2 ml of a Krebs–Henseleit buffer (11 mM Na_2HPO_4, 122 mM NaCl, 3.1 mM KCl, 0.4 mM KH_2PO_4, 1.2 mM $MgSO_4$, 1.3 mM $CaCl_2$; pH 7.4, supplemented with 5.5 mM D-glucose at 37 ºC, followed by incubation in the presence of 5 µCi/ml of D-[3-^{3}H] glucose in fresh Krebs-Henseleit buffer (2 ml) in glass 25-ml Erlenmeyer flasks equipped with a central well containing a tube with 0.5 ml of water. The flask atmosphere was gassed with a O_2/CO_2 (95/5) mixture for 20 s and stopped with a rubber cap, and the flasks were incubated in a thermostatized orbital shaker (Forma Benchtop Orbital Shaker, Model 420, Thermo Fischer) for 4 hours at 37°C. In preliminary experiments (data not shown), we observed that $3H_2O$ collected in the tube placed in the central well was linear with time at least up to 4 hours. Incubations were finished by injecting 0.2 ml of 20 % (v/v) $HClO_4$ (Merck Millipore) through the rubber cap, and flasks were further incubated for 72 h to allow the equilibration of ^3H_2O between the incubation medium and the water

of the central well. The rate of glycolysis was expressed as nmol of D-[3-^{3}H] glucose converted into $^{3}H_2O$ per hour and per mg tissue.

Lactate concentration. Lactate concentrations were measured in the buffer after the 4h incubation period spectrophotometrically by determining the increments in absorbance at 340 nm in a mixture containing 1 mM NAD^+ and 22.5 U/ml lactate dehydrogenase in 0.25 M glycine/0.5 M hydrazine/1 mM EDTA buffer at pH 9.5.

Amino acid decarboxylation rate. Amino acid oxidation rate was measured by assessing the rate of conversion of L-[^{14}C(U)] amino acid mixture [NEC850E050UC, Perkin Elmer] into $^{14}CO_2$. Briefly, heart slices (5-10 mg) were pre-incubated for 30 min in 2 ml of a Krebs–Henseleit buffer (11 mM Na_2HPO_4, 122 mM NaCl, 3.1 mM KCl, 0.4 mM KH_2PO_4, 1.2 mM $MgSO_4$, 1.3 mM $CaCl_2$; pH 7.4, supplemented with 5.5 mM D-glucose at 37 ºC, followed by incubation in the presence of 0.25 µCi/ml of amino acid mixture L-[^{14}C(U)] in fresh Krebs-Henseleit buffer (2 ml) in glass 25-ml Erlenmeyer flasks equipped with a central well containing a tube with 0.5 ml of benzethonium hydroxide (Sigma) for $^{14}CO_2$ equilibration. The flask atmosphere was gassed with a O_2/CO_2 (95/5) mixture for 20 s and stopped with a rubber cap, and the flasks were incubated in a thermostatized orbital shaker (Forma Benchtop Orbital Shaker, Model 420, Thermo Fischer) for 3 hours at 37°C. In preliminary experiments (data not shown), we observed that $^{14}CO_2$ collected in the tube placed in the central well was linear with time at least up to 3 hours. Incubations were then terminated by the addition of 0.2 ml 20% (v/v) perchloric acid (Merck Millipore) for 30 min before the benzethonium hydroxide (containing $^{14}CO_2$) was removed, and the radioactivity was measured with a liquid scintillation analyzer (Tri-Carb 4810 TR, PerkinElmer). Amino acid oxidation rate was expressed as nmol of L-[14C(U)] amino acid mixture converted into $^{14}CO_2$ per hour per mg tissue.

Protein digestion of mouse heart samples. Neonatal mouse heart samples were homogenized using a FastPrep-24 instrument (MP Biomedicals, Illkirch, France), following manufacturer's instructions, in the presence of 50 mM Tris-HCl pH 6.8, 2% SDS and 50 mM DTT, and the resulting solution was boiled for 5 min at 95 ºC. The tissue lysates were centrifuged at 13,000 g for 15 min to remove debris, and protein concentration in the supernatant was determined using the RCDC Protein Assay Kit (Bio-Rad). Protein samples (100 µg) were mixed with denaturing buffer (8 M urea in 100 mM Tris-HCl pH 8.5) and concentrated on 30 K FASP filters (Expedeon). After washing with denaturing buffer at 10,000 rpm for 15 min, free thiol groups were alkylated by incubation with 50 mM iodoacetamide 30 min at room temperature in the dark. Then the filters were washed with denaturing buffer followed by washing with trypsin digestion buffer (50 mM ammonium bicarbonate pH 8.8). Protein samples were digested overnight at 37ºC with sequencing grade trypsin (Promega, Madison, WI, USA) at 1:40 (w/w) trypsin:protein ratio in digestion buffer. The resulting tryptic peptides from each sample were recovered by centrifugation at 10,000 rpm for 5 min after addition of 40 µl of trypsin digestion buffer, after which 50 µl of 500 mM NaCl were added and the filters centrifuged for 15 min at 10,000 rpm. Trifluoroacetic acid was added to a final concentration of 1% and the peptides were desalted on C18 Oasis HLB extraction cartridges (Waters Corporation, Milford, MA, USA) and dried-down.

Isobaric labeling of peptides using Tandem Mass Tags (TMT). The dried peptides were dissolved in triethylammonium bicarbonate buffer, and their concentration was determined using a Direct Detect IR spectrometer (Millipore). Equal amounts of each peptide sample were labeled with isobaric 10-plex Tandem Mass Tags (TMT, Thermo Scientific) according to the manufacturer's instructions and mixed together. Samples were desalted using C18 Oasis HLB extraction cartridges (Waters) and dried-down for later LC-MS/MS analysis.

LC-MS/MS analysis. Peptide samples were taken up in 0.1% formic acid and applied to an EASY-nLC 1000 nano-flow HPLC system (Thermo Fisher Scientific) coupled on-line with an orbitrap Fusion mass spectrometer (Thermo Fisher Scientific). C18-based reverse phase separation was used with a 2-cm trap column and a 50-cm analytical column (EASY-Spray, Thermo Fisher Scientific). Peptides were loaded in buffer A (0.1% formic acid (v/v)) and eluted with a 300-min linear gradient of buffer B (90% ACN, 0.1% formic acid (v/v)) at 200 nL/min flow. Mass spectra were acquired in a data-dependent manner, with an automatic switch between MS and MS/MS, using a top-speed method and 30 s dynamic exclusion. MS spectra were acquired in the 400–1500 m/z range at 120,000 resolution, while HCD MS/MS were performed at 33 normalized collision energy and analyzed with 35,000 resolution in the orbitrap.

Peptide identification. LC-MS/MS data were analyzed with Proteome Discoverer (version 2.1, Thermo Fisher Scientific) using SEQUEST-HT (Thermo Fisher Scientific) against a Uniprot database containing all sequences from Mus musculus (January 2021; 63,700 entries). Database search parameters were selected as follows: trypsin digestion with two maximum missed cleavage sites, precursor mass tolerance of 800 ppm, fragment mass tolerance of 0.02 Da. Met oxidation was considered a variable modification, while Cys carbamidomethylation and Lys and peptide N-terminal modification of +229.163 were set as fixed modifications. The corresponding inverted protein sequences were incorporated to the database for false discovery rate (FDR) calculation. Peptide identification from MS/MS data was performed using the probability ratio method[57], and the FDR of peptide identifications was calculated using the refined method [58,59], taking 1% FDR as a threshold for peptide identification. Peptides were assigned only to the best protein proposed by the Proteome Discoverer algorithm.

Peptide and protein quantification. The quantitative information extracted from the MS/MS spectra by Proteome Discoverer was integrated from the spectrum level to the peptide level and then to the protein level on the basis of the WSPP model[60] and the systems biology triangle algorithm[61] using the SanXoT software package[62]. Briefly, in every scan the $x_{qps} = \log_2 A/B$ was calculated using the TMT reporter ion intensities coming from samples A and B. The statistical weight w_{qps} of each scan was calculated as described in[60]. The log2-ratio of every peptide (x_{qp}) was calculated as the weighted average of its scans, whereas the quantification of each protein (x_p) was the weighted average of its peptides, and the grand mean ($\bar{x}$) as the weighted average of all the protein values[60]. Peptide and protein quantification weights (w_{qp} and w_q, respectively) were calculated from the corresponding scan weights and the peptide variance (σ_P^2) or the peptide

weights and the protein variance (σ_Q^2), respectively[60]. The standardized variable at the peptide level, z_{pq}, was calculated as:

$$z_{pq} = \left(x_{pq} - x_q\right) * \sqrt{w_{pq}} * \sqrt{\frac{n_p}{n_p - 1}}, \qquad n_p>1 \quad \text{(Eq.1)},$$

expressing the deviation between the log2-ratio quantifications of the peptide *p* coming from the protein *q*, quantified with n_p peptides. Similarly, the standardized variable at the protein level, z_q, was calculated as:

$$z_q = \left(x_q - \bar{x}\right) * \sqrt{w_q} * \sqrt{\frac{n_q}{n_q - 1}}, \; n_q>1 \qquad \text{(Eq.2)},$$

where n_q is the number of quantified proteins in the whole experiment. The validity of the null hypothesis was carefully checked at every level (spectrum, peptide and protein) by plotting the cumulative distributions with zero mean and unit variance[60]. Outliers at the peptide and protein levels were detected at 1% FDR as described in[60].

Quantification of protein function. The proteins quantified were functionally annotated using the Gene Ontology[63] database. Quantitative assessment of protein function between samples was carried out using SanXoT as described[62].

RNA-sequencing and analysis. Briefly, total RNA was prepared with RNeasy Mini kit (Qiagen) by standard protocols (#74104, Qiagen RNeasy mini Kit) from 4 biological replicates. cDNA was synthetized and amplified from total RNA (1-10 ng) using the Ovation® RNA-seq System v2 (NuGEN® Technologies. Sequencing was performed using the Illumina HiSeq-2500 system (1x50 8M reads). Transcript abundances were quantified with the Ensembl GRCh38 cDNA reference using RSEM. The expression matrix was filtered for only transcripts with greater than 5 TPM in replicates. Only genes with at least 1 count per million in the 3 or 4 replicates were considered for statistical analysis. Differential expression statistics between KO and Control were generated using limma with TMM normalization. Genes with a Benjamini–Hochberg adjusted p value <0.05 and a cut-off of 0.6 in logFC were considered differentially expressed (DEGs). GO term enrichment was performed using Panther (http://pantherdb.org) applying Bonferroni and Ingenuity analysis (IPA, Qiagen). Heatmaps and Volcano plots were built using RStudio (version 1.2.5033). These experiments were performed at the CNIC Genomics and Bioinformatics Units. Data availability: GSE188998. Refer to Supplemental File 1.

ChIP-sequencing. Chromatin immunoprecitation followed by high throughput sequencing (ChIP-seq) was performed in individual P0 hearts. Each heart was extracted, washed twice in cold PBS 1X and resuspended in 10ml PBS 1X supplemented with cOmplete EDTA-free protease inhibitor [05056489001, Roche]. The whole tissue was fixed with 1% formaldehyde (#28906, ThermoFisher Scientific) for 15 min at RT and gently balance. Reaction was quenched with 125mM Glycine for 5 min at RT followed by two PBS 1X washes. Fixed heart was resuspended in 1 ml of Heart buffer (10mM Tris-HCl pH 7.5, 1mM EDTA, 0.5% SDS, 0.2% Triton X-100),

minced and incubated in a rotator for 30 min at RT. Mixture was next transferred to pre-chilled 1ml AFA tube (Covaris) and sheared in a S220 Focused-ultrasonicator (Covaris) for 20 min (Duty 10%, Cycle 200, PIP 140 and cycle/time 20 seg). After sonication, chromatin was diluted 1:1 in ChIP dilution buffer (0.01% SDS, 1.1% Triton X-100, 1.2 mM EDTA, 16.7 mM Tris-HCl pH 8, 167 mM NaCl, cOmplete EDTA-free protease inhibitor) and 20 µl were removed and kept as input. For immunoprecipitation, the remaining chromatin volume was incubated with either 5 µl H3K27ac antibody (#39135, ActiveMotif, 1:400) or 5µl pan-RXR antibody (#21218-1-AP, ProteinTech, 1:400) in a rotator at 4ºC O/N. Next day, 50 µl of Dynabeads A (#10001D, ThermoFisher Scientific) were washed twice with 2xvolume of cold ChIP dilution buffer, resuspended in the initial volume added to chromatin+antibody mixture. After 2h, beads were washed 5 times with RIPA buffer (50 mM HEPES-KOH pH 7.5, 500 mM LiCl, 1 mM EDTA, 1% NP-40, 0.7% Na-Deoxycholate) and 1 time with Final wash buffer (1xTris-EDTA, 50 mM NaCl). Each wash consisted of 1ml of buffer for 2 min in the cold-room rotator. Next, beads were resuspended in 205 µl of fresh Elution buffer (50 mM Tris-HCl pH 8, 10 mM EDTA, 1% SDS) and incubated at 55ºC 30 min. 200 µl of eluated were moved to a DNA lo-bind tube and 32 µl of Reverse Crosslinking buffer (250 mM Tris-HCl pH 7.5, 32.5 mM EDTA pH 8, 1.25M NaCl, 5 mg/ml Proteinase K) were added and incubated at 65ºC O/N. Input was completed with 180 µl molecular biology water and treated in the same way. DNA was purified using ChIP Clean and Concetrator Zymo kit (#D5201, Zymo Research). DNA concentration and size distribution were checked with Qbit dsDNA HS Assay kit (ThermoFischer Scientific) and Bioanalyzer DNA High Sensitivity Kit (Agilent), respectively. Libraries were prepared according standard protocols and sequenced in HiSeq 3000 (Illumina) with an average of 20 million single-end reads per sample. Data availability: GSE188998.

ChIP-seq processing and analysis. Sequencing reads were pre-processed with Cutadapt v1.7.1[64] to remove adaptor remains. Pre-processed reads were mapped against reference genome mm10 with a pipeline that used BWA 0.7.10 as aligner[65], Piccard to mark duplicate alignments (http://picard.sourceforge.net), and samtools v0.1.18[66] to eliminate multi-mapped alignments. Only mapped reads were kept. Alignments against the mitochondrial genome or chromosomes X and Y were also removed. Once filtered alignments had been obtained, ChIP peaks were called with MACS2 v2.1.1[67], using parameter "-q 0.05" as the false discovery rate cut-off, using ChIP and control files as input. Next, filtered alignments and peaks were processed with the R package DiffBind[68,69] to define a consensus set of peaks, to calculate and normalize their coverage in all samples, and to identify differentially occupied regions, using EdgeR[70] as analysis method. UCSC genome browser was used for visualization of ChIP-seq reads in selected genomic regions. The overlap between ATACseq and ChIPseq peaks was tested with bedtools v2.24.0,[71]and motif enrichment analyses were performed with HOMER v4.10.3[72]. Refer to Supplemental File 1.

ATAC-sequencing in neonatal hearts. Chromatin accessibility experiments were performed according B.Ren ENCODE ATAC-seq protocol (https://www.encodeproject.org/experiments/ENCSR451NAE/) with minor modifications. Briefly,

P0 hearts from edKO and Control mice were processed individually. Cardiac tissue was pulverized with liquid N_2. 10 mg pulverized tissue was resuspended in 1 ml NPB buffer (5%BSA, [#A7906, Sigma]; 0.2% IGEPAL [#I8896, Sigma], 1mM DTT [#D9779, Sigma], 1xcOmplete EDTA-free protease inhibitor [05056489001, Roche] in PBS1X) and rotated for 10 min at 4ºC. Nuclei suspension was filtered using a 30 µm CellTrics (25004-0042-2316, Sysmex) and spin down for 5 min at 500g at 4ºC. Nuclei were resuspended in TB buffer (33mM Tris-acetate pH 7.8 [#BP-152, ThermoFisher Scientific], 66 mM K-Acetate [#P5708, Sigma], 11 mM Mg-Acetate [#M2545, Sigma], 16% DMF [#DX1730, EMD Millipore] in molecular biology water) and nuclei concentration was quantified using and hemocytometer and Trypan Blue stain (#15250061, Thermo Fisher Scientific). Nuclei concentration was adjusted to 50000 nuclei/µl with TB Buffer. Transposase reaction was performed by mixing 10 µl nuclei solution (50000 total nuclei) and 0.5 µl Tagment DNA Enzyme 1 (FC-121-1030, Illumina) and incubated 30 min with 500 rpm at 37ºC. Tagmented DNA was purified using MinElute PCR Purification Kit (#28004,Qiagen) and eluted in 10 µl EB. For library preparation, barcodes were added by mixing 10 µl tagmented DNA, 11 µl NEBNext 2x PCR Master mix (#M0541), 0.2µl Primer Ad1_noMx 100 µM (Forward), 0.2 µl Ad2.X 100 µM (Reverse, different for each sample), 0.6 µl molecular biology water and with the following PCR programme: 72ºC 5 min, 98ºC 30 seg, 8 cycles (98ºC 10 seg, 63ºC 30 seg, 72ºC 1 min). Primers were obtained in[21]. PCR product was again purified with MinElute PCR Purification Kit (#28004,Qiagen) and eluted in 50 µl EB. We next performed 0.65x size selection followed by 1.5x clean-up with AMPure XP beads (#A63880, Beckman Coulter). Depending on library concentration, additional PCRs cycles (98ºC 30 seg, (98ºC 10 seg, 63ºC 30 seg, 72ºC 1 min) 5-8 cycles depending on the sample) were perfomed. Libraries were purified with AMPure XP beads, and concentration was measured by the Qbit dsDNA HS Assay kit (ThermoFischer Scientific) and fragment profiles were analysed with the Bioanalyzer DNA High Sensitivity Kit (Agilent). Libraries were sequenced on 2×50 HiSeq 3000 (Illumina) and with an average of 25 million paired-end reads per sample. Data availability: GSE188998.

ATAC-seq processing and analysis. Cutadapt v1.7.1 was used to trim adaptors (http://journal.embnet.org/index.php/embnetjournal/article/view/200). Trimmed paired-end reads were aligned to the mm10 mouse reference genome using Bowtie2 v4.1.2[73] with settings -X 2000 -very-sensitive in paired-end mode. Duplicates were marked with PICARD tools (http://picard.sourceforge.net). Reads were subsequently filtered for alignment quality (>Q30) and were required to be properly paired.Duplicates and reads mapping to the mitochondria, unmapped contigs or chromosomes X and Y were removed. Secondary alignments were not considered. ATAC-seq peaks were called using MACS2 v2.1.1[74] with parameters -nomodel -shift 100 -extsize 200 -keep-dup all -pval 0.001. Peaks falling within mouse mm10 ENCODE blacklisted regions (http://mitra.stanford.edu/kundaje/akundaje/release/blacklists/mm10-mouse) were discarded using bedtools v2.24.0 intersect. A consensus peak set of peaks detected in at least two samples was generated using function dba.counts from DiffBind R package v2.6.6 (http://bioconductor.org/packages/release/bioc/htmL/DiffBind.htmL). EdgeR v3.20.9[70] was used to perform a differential accessibility analysis on the set of consensus peaks using Diffbind

functions (dba.analyze). Control-increased chromatin accesibility regions were defined by log2 fold change in read density > 1 and adj. *P* value <0.05. Conversely, edKO-increased chromatin accessibility regions were defined by log2 fold change <−1 and adj. *P* value < 0.05. Differentially accessible peaks were associated to the gene with the nearest TSS using command annotatePeaks.pl from the HOMER v4.10.3[72]. UCSC genome browser was used for visualization of ATAC-seq reads in selected genomic regions. Transcription factor motif enrichment analyses for genomic regions showing differential accessibility were performed using HOMER command findMotifsGenome.pl. edKO peaks with increased accessibility were compared to control peaks and viceversa. Refer to Supplemental File 1.

GC-MS metabolomics. Neonatal hearts were excised and frozen in liquid N_2. Similar amounts were added to 100 µl of cold methanol (MetOH) 100% and homogenated using a TissueLyser (Qiagen) -3.8 (1 ball) 50 Hz speed for 5 min. Metabolite extraction, derivatization, instrumental analysis and data analysis were performed as recently described[75]. For metabolite extraction, 50 µl homogenate were mixed with 100µl MeOH 100% in a vortex for 20 min at RT and centrifuged at 4000g for 20 min at RT. 50 µl of supernatant were taken and dried in Speedvac. For derivatization first step, 20 µl of O-methoxyamine HCL in pyridine was added, ultrasonicated (2 min, 3 cycles), vortexed for 5 min and incubated in darkness at RT for 16h. Derivatization step 2 consisted of vortexing for 5 min with 20 µl of BSTFA, 1h incubation at 70ºC and cool-down in the darkness for 30 min. Next, 100 µl of 10 ppm IS was incorporated and centrifuged for 15min at 700g at RT. The analysis was performed with an GC instrument (7890 A) coupled to an inert mass spectrometer with Triple-Axis Detector (5975C), both from Agilent Technologies (Santa Clara CA, USA). Data were acquired using the Agilent MSD ChemStation Software. Deconvolution and metabolite identification of raw data collected by GC-MS analysis were performed by Agilent MassHunter Unknowns Analysis Tool 7.0. A chemical identity was assigned to the compounds by the software by searching in two target libraries: Fiehn library and NIST (National Institute of Standards and Technology) B09.0 2017. Data were aligned using Agilent MassProfiler Professional 13.1 and integration was performed with Agilent MassHunter Quantitative. The raw data collected by GC-MS was cleaned of background noise with Microsoft Excel (2016). To keep only metabolites with a good repeatability only features with RSD <25% in QC were evaluated as relevant. Data was normalized by the Total Useful Signal (TUS). For univariate analysis, differences between groups (edKO vs Control) for GC-MS analysis were evaluated for individual metabolites using univariate statistical analysis after log_2 transformation of the data and normalization by TUS. Unpaired t-test with Bonferroni FWER were performed with Mass Profiler Professional 13.1.

In silico ligand docking analysis. Fasta sequences of mouse RXRa (Uniprot ID P28700) was aligned to Uniclust·30 (release 08-2018) and pdb70 (release 09-2019) databases using the hhblits/hhsearch tools of the HH-suite3[76] to obtain a multisequence alignment (MSA) and pdb templates for comparative modeling. For docking the monomer, a comparative modeling was made using de RosettaCM[77] tool of the of Rosetta suite v3.12 (www.rosettacommons.org) with the fasta sequence, the alignment and templates obtained before. The models obtained were

clustered using the cluster tool of Rosetta suite v3.12 (www.rosettacommons.org) and the bigger clusters were selected. A multi structural alignment (MSTA) of the models selected with the templates was made using the mTMAlign tool[78,79]. The model with best structural alignment to the templates was selected as final candidate. A final cycle of refinement for minimize clashes and energy was made with the relax tool[80,81]of Rosetta suite v3.12 (www.rosettacommons.org). At least, 100 independent models were calculated. The model with correct topology and minimal score was selected as final model. To model the dimer form of rxra, a MSTA of the model obtained before and 4nqaAH.pdb structure to generate a template and a symmetric restrictions file (order 2) for docking the dimer using the symmetric docking protocol of Rosetta suite v3.12 (www.rosettacommons.org). Models with positive energy were cut-off and filtered models were clustered as before and the bigger cluster was MSTA using the MMAlign tool [82]. The model with best MSTA to template was selected as final model. To evaluate energy of the complex and the interface, the model was analyzed with the InterfaceAnalyzer tool of Rosetta suite v3.12 (www.rosettacommons.org). To compare the effect of different ligands GLA and Dihomo-gamma-linolenic acid (DGLA), the complex of each one with the models of rxra homodimer modelled before were docked with the ligand-docking tool using the Rosetta script [83,84] of the Rosetta software suite v3.12. Briefly, a representative conformer of the ligand was located close to the ligand pocket in chain A of the receptor complex rxra dimer (MSTA to 1fm9). The protocol compute combinations of atomic coordinates for conformers of ligand and rearrangement of the sidechain (rotamers) of the residues of the receptor to explore the conformational space to find interactions between ligand and protein. In all cases, at least 1000 models were computed and the model with correct interface topology (ligand inside the pocket without clashes between ligand and protein) and best energy interface (minor ΔG, more stability and interactions between protein and ligand like electrostatic, hydrophobic/hydrophilic, van der Waals and hydrogen bonds or salt bridges) was selected. A final cycle of refinement for minimize clashes and energy was made with the relax tool. At least, 100 independent models were calculated for each one. As before, the model with correct topology and minimal score was selected as final model candidate. The protocol before was repeated with a new ligand residue in the second pocket in chain B for each model candidate to obtain final models.

Luciferase assays. For transient transfection, 80.000 cells HEK293.T cells (kindly donated by Dr. Thierry Fischer) were seeded and transfected with jetPEI transfection reagent (Polyplus) following manufacturer´s instructions. We transfected $(AOX)_3$-TK or UAS-TK luciferase reporters together with expression plasmids for human-RXRα, human-RXRα-ΔAF2, GAL4-RXRα, GAL4-RXRα-ΔAF2, coactivator SRC1 or pCMX empty vector, as a negative control. GAL4 constructs were kindly provided by Dr. John S. Welch[35]. After a transient transfection of 6 hours, cells were treated with LG268 (1 µM), GLA-BSA-conjugated (500 µM), or UVI3003 (1 µM) together with 500 µM GLA-BSA-conjugated, for 24h hours. Luciferase activity was measured with Luciferase Assay System (Promega).

Protein expression and purification. Non-liganded recombinant human RXRα-LBD (residues 223-462) cloned into a pET15b expression vector was expressed in BL21 (DE3) bacterial strain

as fusion proteins with an N-terminal hexahistidine (His) tag and purified to homogeneity using standard chromatographic procedures[85]. Cells were grown in LB medium and induced overnight with 1 mM isopropyl-beta-D-thiogalactopyranoside (IPTG) at 16ºC. The purification procedure included two sequential affinity chromatography steps using a niquel chelating column. His tag was removed using thrombin digestion overnight during dialysis. Protein samples contained 20 mM HEPES, 500 mM NaCl, 10% glycerol, 75 mM imidazole, 1 mM DTT at pH 8.0. SDS-PAGE gels assessed purity and homogeneity of protein samples.

Surface plasmon resonance (SPR) analysis. SPR analyses were performed at 25°C in a BIAcore T200 instrument (GE Healthcare). Highly purified, recombinant and unliganded RXRα-LBD protein was diluted in 10 mM sodium acetate pH 5.0, and directly immobilized as ligand on CM5 chips (GE Healthcare) by amine coupling at a density of 4000 resonance units (RU). As a reference, one of the channels was also amine-activated and blocked in the absence of protein. The running buffer was 1x PBS, 5% DMSO, 0.05% Tween. The compound GLA and an SRC3-2 coactivator derived-peptided were used as analyte and injected in solution over the immobilized protein sample. Sensorgrams were analyzed with the BIAcore T200 Evaluation software 3.0 and fitted according to the Langmuir 1:1 model.

Statistical analysis. Data are presented as means ± s.e.m. Unpaired t-test was used when two groups were compared, and comparison of more than two datasets was done using one-way analysis of variance (ANOVA) with Tukey's post-test. When indicated, Benjamini hochberg correction was applied to correct multiple-testing per genes. Comparisons of two-time curves or datasets were performed using two-way ANOVA followed by Tukey's post-test. For blood lactate and glucose determinations, non-parametric Kruskal-Wallis (Dun´s correction) was applied. All statistical analyses were performed using Prism v7 (GraphPad Software, California, USA). Differences were considered significant when $p < 0.05$, and represented as $*P < 0.05$, $**P < 0.01$, $***P < 0.001$, and $****P < 0.0001$. Sample exclusion was not performed unless statistically significant outliers were identified using Grubb's test (ESD method).

Data availability. Data generated from RNA-seq, ATAC-seq, ChIP-seq have been deposited in the Gene Expression Omnibus with the accession number GSE18899. Source data for main and Extended Data Figures are available online as separate Excel files for each figure. Lipidomics raw data from cardiac tissue (Fig.2d) and milk (Fig.4h) can be found in Supplementary Table 1 and Supplementary Table 2, respectively.

Additional references

36 Kastner, P. *et al.* Abnormal spermatogenesis in RXR beta mutant mice. *Genes & development* **10**, 80-92, doi:10.1101/gad.10.1.80 (1996).

37 Mascrez, B., Ghyselinck, N. B., Chambon, P. & Mark, M. A transcriptionally silent RXRalpha supports early embryonic morphogenesis and heart development. *Proceedings of the National Academy of Sciences of the United States of America* **106**, 4272-4277, doi:10.1073/pnas.0813143106 (2009).

38 Subbarayan, V. *et al.* RXRalpha overexpression in cardiomyocytes causes dilated cardiomyopathy but fails to rescue myocardial hypoplasia in RXRalpha-null fetuses. *The Journal of clinical investigation* **105**, 387-394, doi:10.1172/jci8150 (2000).

39 Merki, E. *et al.* Epicardial retinoid X receptor alpha is required for myocardial growth and coronary artery formation. *Proceedings of the National Academy of Sciences of the United States of America* **102**, 18455-18460, doi:10.1073/pnas.0504343102 (2005).

40 Leone, T. C., Weinheimer, C. J. & Kelly, D. P. A critical role for the peroxisome proliferator-activated receptor alpha (PPARalpha) in the cellular fasting response: the PPARalpha-null mouse as a model of fatty acid oxidation disorders. *Proceedings of the National Academy of Sciences of the United States of America* **96**, 7473-7478, doi:10.1073/pnas.96.13.7473 (1999).

41 Cardoso, A. C. *et al.* Mitochondrial substrate utilization regulates cardiomyocyte cell-cycle progression. *Nature Metabolism* **2**, 167-178, doi:10.1038/s42255-020-0169-x (2020).

42 Chinen, Y. *et al.* A novel homozygous missense SLC25A20 mutation in three CACT-deficient patients: clinical and autopsy data. *Human Genome Variation* **7**, 11, doi:10.1038/s41439-020-0098-y (2020).

43 Mychaleckyj, J. C. *et al.* Association of breast milk gamma-linolenic acid with infant anthropometric outcomes in urban, low-income Bangladeshi families: a prospective, birth cohort study. *European Journal of Clinical Nutrition* **74**, 698-707, doi:10.1038/s41430-019-0498-6 (2020).

44 Li, M. *et al.* Retinoid X receptor ablation in adult mouse keratinocytes generates an atopic dermatitis triggered by thymic stromal lymphopoietin. *Proceedings of the National Academy of Sciences of the United States of America* **102**, 14795-14800, doi:10.1073/pnas.0507385102 (2005).

45 Cruz-Adalia, A. *et al.* CD69 limits the severity of cardiomyopathy after autoimmune myocarditis. *Circulation* **122**, 1396-1404, doi:10.1161/circulationaha.110.952820 (2010).

46 Ram, R., Mickelsen, D. M., Theodoropoulos, C. & Blaxall, B. C. New approaches in small animal echocardiography: imaging the sounds of silence. *American journal of physiology. Heart and circulatory physiology* **301**, H1765-1780, doi:10.1152/ajpheart.00559.2011 (2011).

47 Koelmel, J. P. *et al.* Lipid Annotator: Towards Accurate Annotation in Non-Targeted Liquid Chromatography High-Resolution Tandem Mass Spectrometry (LC-HRMS/MS) Lipidomics Using a Rapid and User-Friendly Software. *Metabolites* **10**, 101 (2020).

48 Tsugawa, H. *et al.* A lipidome atlas in MS-DIAL 4. *Nature Biotechnology* **38**, 1159-1163, doi:10.1038/s41587-020-0531-2 (2020).

49 Ortega-Senovilla, H., Schaefer-Graf, U. & Herrera, E. Pregnant women with gestational diabetes and with well controlled glucose levels have decreased concentrations of individual fatty acids in maternal and cord serum. *Diabetologia* **63**, 864-874, doi:10.1007/s00125-019-05054-x (2020).

50 Alonso-Herranz, L. *et al.* Macrophages promote endothelial-to-mesenchymal transition via MT1-MMP/TGFβ1 after myocardial infarction. *Elife* **9**, doi:10.7554/eLife.57920 (2020).

51 Li, Z., Ross Stewart, K. M., Bruton, F. A., Denvir, M. A. & Brittan, M. in *Angiogenesis: Methods and Protocols* (ed Andrew V. Benest) 297-309 (Springer US, 2022).

52 Quiros, P. M., Goyal, A., Jha, P. & Auwerx, J. Analysis of mtDNA/nDNA Ratio in Mice. *Current protocols in mouse biology* **7**, 47-54, doi:10.1002/cpmo.21 (2017).

53 Fernandez-Vizarra, E., Lopez-Perez, M. J. & Enriquez, J. A. Isolation of biogenetically competent mitochondria from mammalian tissues and cultured cells. *Methods (San Diego, Calif.)* **26**, 292-297, doi:10.1016/s1046-2023(02)00034-8 (2002).

54 Bradford, M. M. A rapid and sensitive method for the quantitation of microgram quantities of protein utilizing the principle of protein-dye binding. *Analytical biochemistry* **72**, 248-254, doi:10.1006/abio.1976.9999 (1976).

55 Vives-Bauza, C., Yang, L. & Manfredi, G. Assay of mitochondrial ATP synthesis in animal cells and tissues. *Methods in cell biology* **80**, 155-171, doi:10.1016/s0091-679x(06)80007-5 (2007).

56 Herrero-Mendez, A. *et al.* The bioenergetic and antioxidant status of neurons is controlled by continuous degradation of a key glycolytic enzyme by APC/C-Cdh1. *Nature cell biology* **11**, 747-752, doi:10.1038/ncb1881 (2009).

57 Martinez-Bartolome, S. *et al.* Properties of average score distributions of SEQUEST: the probability ratio method. *Molecular & cellular proteomics : MCP* **7**, 1135-1145, doi:10.1074/mcp.M700239-MCP200 (2008).

58 Navarro, P. & Vazquez, J. A refined method to calculate false discovery rates for peptide identification using decoy databases. *J Proteome Res* **8**, 1792-1796, doi:10.1021/pr800362h (2009).

59 Bonzon-Kulichenko, E., Garcia-Marques, F., Trevisan-Herraz, M. & Vazquez, J. Revisiting peptide identification by high-accuracy mass spectrometry: problems associated with the use of narrow mass precursor windows. *J Proteome Res* **14**, 700-710, doi:10.1021/pr5007284 (2015).
60 Navarro, P. *et al.* General statistical framework for quantitative proteomics by stable isotope labeling. *Journal of proteome research* **13**, 1234-1247, doi:10.1021/pr4006958 (2014).
61 Garcia-Marques, F. *et al.* A Novel Systems-Biology Algorithm for the Analysis of Coordinated Protein Responses Using Quantitative Proteomics. *Mol Cell Proteomics* **15**, 1740-1760, doi:10.1074/mcp.M115.055905 (2016).
62 Trevisan-Herraz, M. *et al.* SanXoT: a modular and versatile package for the quantitative analysis of high-throughput proteomics experiments. *Bioinformatics*, doi:10.1093/bioinformatics/bty815 (2018).
63 The Gene Ontology, C. The Gene Ontology Resource: 20 years and still GOing strong. *Nucleic Acids Res* **47**, D330-D338, doi:10.1093/nar/gky1055 (2019).
64 Martin, M. Cutadapt removes adapter sequences from high-throughput sequencing reads. *EMBnet.journal* **17**, 10-12 (2011).
65 Li, H. & Durbin, R. Fast and accurate short read alignment with Burrows-Wheeler transform. *Bioinformatics* **25**, 1754-1760, doi:10.1093/bioinformatics/btp324 (2009).
66 Li, H. *et al.* The Sequence Alignment/Map format and SAMtools. *Bioinformatics* **25**, 2078-2079, doi:10.1093/bioinformatics/btp352 (2009).
67 Zhang, Y. *et al.* Model-based Analysis of ChIP-Seq (MACS). *Genome Biology* **9**, R137, doi:10.1186/gb-2008-9-9-r137 (2008).
68 Ross-Innes, C. S. *et al.* Differential oestrogen receptor binding is associated with clinical outcome in breast cancer. *Nature* **481**, 389-393, doi:10.1038/nature10730 (2012).
69 Stark, R. & Brown, G. (2011). DiffBind: differential binding analysis of ChIP-Seq peak data.
70 Robinson, M. D., McCarthy, D. J. & Smyth, G. K. edgeR: a Bioconductor package for differential expression analysis of digital gene expression data. *Bioinformatics (Oxford, England)* **26**, 139-140, doi:10.1093/bioinformatics/btp616 (2010).
71 Quinlan, A. R. & Hall, I. M. BEDTools: a flexible suite of utilities for comparing genomic features. *Bioinformatics* **26**, 841-842, doi:10.1093/bioinformatics/btq033 (2010).
72 Heinz, S. *et al.* Simple combinations of lineage-determining transcription factors prime cis-regulatory elements required for macrophage and B cell identities. *Molecular cell* **38**, 576-589, doi:10.1016/j.molcel.2010.05.004 (2010).
73 Langmead, B. & Salzberg, S. L. Fast gapped-read alignment with Bowtie 2. *Nature methods* **9**, 357-359, doi:10.1038/nmeth.1923 (2012).
74 Zhang, Y. *et al.* Model-based analysis of ChIP-Seq (MACS). *Genome biology* **9**, R137, doi:10.1186/gb-2008-9-9-r137 (2008).
75 Rey-Stolle, F. *et al.* Low and high resolution gas chromatography-mass spectrometry for untargeted metabolomics: A tutorial. *Analytica Chimica Acta*, 339043, doi:https://doi.org/10.1016/j.aca.2021.339043 (2021).
76 Steinegger, M. *et al.* HH-suite3 for fast remote homology detection and deep protein annotation. *BMC Bioinformatics* **20**, 473, doi:10.1186/s12859-019-3019-7 (2019).
77 Song, Y. *et al.* High-resolution comparative modeling with RosettaCM. *Structure* **21**, 1735-1742, doi:10.1016/j.str.2013.08.005 (2013).
78 Dong, R., Pan, S., Peng, Z., Zhang, Y. & Yang, J. mTM-align: a server for fast protein structure database search and multiple protein structure alignment. *Nucleic acids research* **46**, W380-w386, doi:10.1093/nar/gky430 (2018).
79 Dong, R., Peng, Z., Zhang, Y. & Yang, J. mTM-align: an algorithm for fast and accurate multiple protein structure alignment. *Bioinformatics (Oxford, England)* **34**, 1719-1725, doi:10.1093/bioinformatics/btx828 (2018).
80 Conway, P., Tyka, M. D., DiMaio, F., Konerding, D. E. & Baker, D. Relaxation of backbone bond geometry improves protein energy landscape modeling. *Protein Sci* **23**, 47-55, doi:10.1002/pro.2389 (2014).
81 Nivón, L. G., Moretti, R. & Baker, D. A Pareto-optimal refinement method for protein design scaffolds. *PLoS One* **8**, e59004, doi:10.1371/journal.pone.0059004 (2013).
82 Mukherjee, S. & Zhang, Y. MM-align: a quick algorithm for aligning multiple-chain protein complex structures using iterative dynamic programming. *Nucleic acids research* **37**, e83, doi:10.1093/nar/gkp318 (2009).

83 Capra, J. A., Laskowski, R. A., Thornton, J. M., Singh, M. & Funkhouser, T. A. Predicting protein ligand binding sites by combining evolutionary sequence conservation and 3D structure. *PLoS Comput Biol* **5**, e1000585, doi:10.1371/journal.pcbi.1000585 (2009).
84 Fleishman, S. J. *et al.* RosettaScripts: a scripting language interface to the Rosetta macromolecular modeling suite. *PLoS One* **6**, e20161, doi:10.1371/journal.pone.0020161 (2011).
85 Egea, P. F. *et al.* Crystal structure of the human RXRα ligand-binding domain bound to its natural ligand: 9-cis retinoic acid. *The EMBO Journal* **19**, 2592-2601, doi:https://doi.org/10.1093/emboj/19.11.2592 (2000).

Acknowledgments. We thank the members of the M.R. and J.A.E laboratories, A. Hidalgo, and M. Torres (all CNIC) for extensive discussions of the paper; G. Sabio (CNIC), N. Rochel (IGBMC), and D. Metzger (IGBMC) for mice and reagents; CNIC and CRG Genomics Units for sequencing; S. Bartlett (CNIC) for editorial assistance; and A.V. Alonso, L. Flores, R. Baeza, R. Santos-Clemente (all CNIC), C. Gifford (Stanford University), and N. Spann (UCSD) for technical assistance. J.P.B. is funded by the NextGenerationEU/PRTR and Agencia Estatal de Investigación (10.13039/501100011033; PID2019-105699RB-I00; PDC2021-121013-I00, RED2018-102576-T), Instituto de Salud Carlos III (CB16/10/00282); and Junta de Castilla y León (Apoyo Regional a la Competitividad Empresarial, ICE 04/18/LE/0017 and Escalera de Excelencia CLU-2017-03). D.J.B. is a recipient of a Juan de la Cierva-Incorporación contract (IJC2020-044230-I). F.J.R is funded by the Ministerio de Ciencia e Innovación (MCIN) and European Regional Development Fund FEDER (PID2021-122490NB-I00). V.A.R.S. received funding from Airbus Defense and Space through the CLX-2 program in partnership with Comando da Aeronautica (COMAER) and the Coordenação de Aperfeiçoamento de Pessoal de Nível Superior-Brasil (CAPES). E.T. received funding from the Swedish Research Council (2020-01150), the Swedish Cancer Society (211582), and the Novo Nordisk Foundation (NNF20OC0063672). J.A.E was supported by RTI2018-099357-B-I00, MCIU/AEI/ ERDF/UE; RTI2018-099357-B-I00 MCIU/AEI; PID2021-1279880B-100 MCIN/AEI /10.13039/501100011033/ERDF,UE; CB16/10/00282 CIBERFES and 17CVD04 Foundation Leducq. This work was supported by grants to M.R.: SAF2017-90604-REDT-NurCaMeIn MINECO/AEI; RTI2018-095928-BI00, MCIU/AEI/ ERDF/UE; PID2021-122552OB-I00 MCIN/AEI /10.13039/501100011033/ERDF,UE; 201605-32 Fundació La Marató de TV3; and S2017/BMD-3684 Comunidad de Madrid/ESF/EU, S2022/BMD-7227 Comunidad de Madrid; and an MINECO fellowship to A.P. (BES-2016-076632). The CNIC is supported by the Instituto de Salud Carlos III (ISCIII), the Ministerio de Ciencia e Innovación (MCIN), and the Pro CNIC Foundation, and is a Severo Ochoa Center of Excellence (grant CEX2020-001041-S funded by MICIN/ AEI/ 10.13039/501100011033).

Declaration of interests. The authors declare no competing interests**.**

Author contributions. Conceptualisation: A.P and M.R.; Performed research: A.P., R.J-M., D.J-B., V.N., I.C., M.V-O., A.A., T.F., A.G., V-A-R.S., Z.H., P.H-A., C.C., and E.C.; Software: F.W., F.M. and F.S-C.; Data interpretation and analysis: A.P., R.J-M, M.V-O., J.V., J.R-C., E.A-G., E.T.,

J-P.B., E.E-P., F-J.R., C.B. J.A.E and M.R.; Writing, reviewing & manuscript editing: A.P., J.A.E., and M.R.; Project supervision: A.P., J.A.E., and M.R.; Funding: M.R.

Extended data Figure 1. **Functional features of edKO mice after birth. (a)** RXRs gene expression (E12.5 (n=5), E14.5 (n=4), E18.5 (n=5), P1 (n=4), P15 (n=4) and P21 (n=3)) in C57Bl6/J hearts. Data as means±s.e.m. **(b)** *Rxra* and *Rxrb* cardiac expression in edKO (n=3-6) and Control (n=4-6) mice. Data as means±s.e.m. Two-way ANOVA. **(c)** Echocardiography parameters in edKO (n=9) and control (n=11) mice (P0). Data as means±s.e.m. Two-tailed Student t test. **(d)** Left, Heart diameter (mm) and right, non-compacted (NC) and compacted (C) myocardial width in E18.5 edKO (n=9) and control (n=8) mice. Data as means±s.e.m. Two-tailed Student t test. **(e)** Thickness (µm) of trabeculae (T) and compact myocardium (CM) in E18.5 edKO (n=9) and control (n=8) mice. Data as means±s.e.m. Paired Two-tailed Student t test. **(f)** Hematoxylin-eosin staining of edKO and control hearts (E18.5). Scale bar=500 µm. **(g)** Heart weight/body weight ratio (%HWBW) (control=17, edKO=15), body weight (g) (control=48, edKO=33), and heart weight (g) (control=17, edKO=14). Data as means±s.e.m. Two-tailed Student t test. **(h)** Electrocardiography parameters in P0 edKO (n=10) and control (n=5) mice. Data as means±s.e.m. Two-tailed Student t test. **(i)** *Rxra* and *Rxrb* expression in tissues from edKO (n=3-6) and control (n=5-6) mice (P0). Data as means±s.e.m. Two-tailed Student t test. **(j)** Suckling score piecharts for 30 control and 15 edKO mice. **(k)** Stress markers expression in control (n=5) and edKO (n=6) lungs (P0). Data as means±s.e.m. Two-tailed Student t test. **(l)** Hematoxylin-eosin staining of edKO and control lungs (P0). Scale bar=500 µm. **(m)** Wet/Dry lung ratio from control (n=16) and edKO (n=9) (P0) mice. Data as means±s.e.m. Two-tailed Student t test. **(n)** Mean, maximum, and minimum body temperature (ºC) in edKO (n=5) and control (n=5) mice at P0. Data as means±s.e.m. Two-tailed Student t test. Exact *P* values in Source Data.

Extended data Figure 2. Cardiac mitochondrial morphology or quantity is not altered in edKO hearts. (a) Fatty acid-derived energy homeostasis pathway. **(b)** Heatmaps and hierarchical clustering of proteomics enrichment data (Zq value edKO vs control hearts) for proteins involved in ROS metabolism, the degradome, mitochondrial dynamics, and the mitochondrial unfolded protein response (mtUPR). **(c)** TEM acquisition of cardiac mitochondria at P0 in control and edKO hearts. **(d)** Left, Mitochondrial area normalized to the cell area in edKO (n=3) and control (n=3) hearts (P0) (arbitrary units). Dots are technical replicates from 3 individual biological replicates/group. Right. Mitochondrial area in edKO (n=3) and control (n=3) hearts (P0). Each dot is one mitochondrion (mean=25-65 mitochondria/3 mice per condition). Data as means±s.e.m. Two-tailed Student t test. **(e)** Mitochondrial copy number (mtDNA/nDNA) in P0 edKO (n=8) and control (n=12) hearts. Data as means±s.e.m. Two-tailed Student t test. **(f)** GC-MS volcano plot in edKO and control hearts (P0). $P_{\text{Aspartic acid}}$=0.00669, P_{Uracil}=0.0249, $P_{\text{Creatinine}}$=0.02812, P_{Glycerol}=0.03959. Log_2FC, log2 fold-change edKO vs control. The dotted line indicates *P* value<0.05. Dot size represents the variable importance parameter (VIP) value. Green and yellow dots represent downregulated and upregulated metabolites, respectively. **(g)** RT-qPCR quantification of *Upp1* in cardiac tissue in edKO (n=3-6) and Control (n=4-6) mice. Data as means±s.e.m. Two-way ANOVA. **(h)** *Ex vivo* rate of amino acid decarboxilation in P0 edKO (n=7)

and control (n=12) hearts, measured as [U-^{14}C] amino acid conversion to $^{14}CO_2$ (nmol x h^{-1}per mg tissue). Data as means ± s.e.m. Two-tailed Student t test. **(i)** a-ketoglutarate (α-KG) quantification (area corrected/signal quantification, arbitrary units) in edKO (n=4) and control (n=4) P0 hearts. Data were presented as means±s.e.m. Two-tailed Student t test. **P*<0.05, ***P* <0.01, ****P* <0.001, *****P* <0.0001. Exact *P* values in Source Data.

Extended data Figure 3. RXRs drive chromatin openness and histone activation of mtFAH signature genes. **(a)** MA plots representing the H3K27ac ChIP-seq data (left) and ATAC-seq data (right) of changes in chromatin activation and openness in edKO perinatal hearts, respectively. X-axis denotes the Log2mean expression for each peak and Y-axis indicates Log_2FC edKO vs control for each peak. Significant (adjusted *P* value <0.05, Log_2FC=0.6) active/open and inactive/closed annotated genes are colored in red and blue, respectively. Two-tailed Student t test (Benjamini-Hochberg correction per gene). Top 20 genes are highlighted in each case. **(b)** Annotation distribution of differentially open peaks (ATAC-seq) and differentially active *loci* (H3K27ac ChIP-seq) in edKO P0 hearts. Total peaks are indicated as well as the percentage of each annotation. **(c)** Relative RT-qPCR quantification of mtFAH genes in cardiac tissue from control (n=5) and PPARα-null (n=5) P0 newborns. Independent biological replicates. Data were presented as means±s.e.m. Two-tailed Student t test. **(d)** Volcano plot depicting the intersection between RNA-seq and H3K27ac ChIP-seq experiments in edKO P0 hearts. Points are plot according Log_2FC and $-log_{10}$(adjusted *P* value) in RNA-seq experiment. Two-tailed Student t test (Benjamini-Hochberg correction per gene). Color and size are plot according Log_2FC and $-log_{10}$(adjusted *P* value) in H3K27ac ChIP-seq experiment, respectively. **(e)** HOMER motif enrichment analysis. Top-scoring motifs in RXR ChIP-seq peaks are shown, together with *P* values, best-match transcription factors, type of direct repeat sequence (DR) and % of target and background sequences. **(f)** Annotation distribution of RXR cistrome in P0 hearts. Total peaks are indicated as well as the percentage of each annotation. **P*<0.05, ***P* <0.01, ****P* <0.001, *****P* <0.0001. Exact *P* values are provided in Source Data.

Extended data Figure 4. Fasting and milk-borne vitamin A effects on the mtFAH gene signature. (a) RXR and mtFAH gene expression in C57Bl6/J hearts treated with vehicle (n=5) or bexarotene (n=5). Data as means ± s.e.m. Two-tailed Student t test (Benjamini-Hochberg). **(b)** Experimental outline for studying the contribution of milk suckling. **(c)** RXR expression from fed (black) or fasted (green) control (n=5-12) and edKO (n=4-6) hearts. Data as means±s.e.m. Two-way ANOVA (Tukey's) **(d)** mtFAH gene expression from fed or fasted control (n=5-12) and edKO (n=4-6) hearts (P0). Data as mean ± s.e.m. Two-way ANOVA (Tukey's). **(e)** RXR and mtFAH gene expression from control (n=10-22) and edKO (n=6-12) newborns (P0) suckled with NCD or vitamin-A-deficient (VAD) milk. Data as means±s.e.m. Two-way ANOVA (Tukey's). **(f)** Metabolic gene expression from NCD (n=6) or FFD (n=11) hearts (P0). Data as mean ± s.e.m. Two-tailed Student t test. **(g)** RXRs gene cardiac expression from control (n=10-17) and edKO (n=12-13) NCD or FFD pups. Data as means±s.e.m. Two-way ANOVA (Tukey). **(h)** Body weight (g) of NCD (n=12) or FFD (n=16) newborns (P1). Data as means±s.e.m. Two-tailed Student t test. **(i)**

Echocardiography parameters in NCD (n=4) and FFD (n=6) newborns. Fractional area change (FAC, %). Data as means±s.e.m. Two-tailed Student t test. **(j)** Body temperature (ºC) in FFD (n=9) and NCD (n=5) mice (P0). Data as means±s.e.m. Two-tailed Student t test. **(k)** Wet/Dry lung ratio from NCD (n=19) and FFD (n=7) (P0) mice. Data as means±s.e.m. Two-tailed Student t test (n=7-19 mice/condition). **(l)** Corrected abundance of total free FAs in NCD (n=6) or FFD (n=4) milk. SAFA, saturated FAs. MUFA, monounsaturated FAs. DUFA, di-unsaturated FAs. PUFA, polyunsaturated FAs. Data as means±s.e.m. Two-tailed Student t test. **(m)** Relative abundance of predominant SAFAs and MUFAs in NCD (n=6) and FFD (n=4) milk. Data as means±s.e.m. Two-tailed Student t test. Exact *P* values in Source Data.

Extended data Figure 5. GLA-RXR activates the expression of mtFAH gene signature. (a) ω-6 fatty acids in vitro stimulation approach. **(b-c)** mtFAH gene expression (% of control) resulting from GLA-BSA (n=4), LA-BSA (n=4), and LG268 (n=4-6) stimulation in primary neonatal cardiomyocytes (nCM) **(b)** or HL1 cell line **(c).** Data as means±s.e.m. Two-tailed Student t-test (ligand vs baseline, Benjamini-Hochberg). Representative experiment (n=3). **(d)** Dose-response curves of GLA-BSA stimulation in nCM (n=3 technical replicates). Representative experiment (n=3). Data as means±s.e.m. Non-linear regression. **(e)** mtFAH gene signature expression in nCM with GLA-BSA (n=10) and GLA-BSA +UVI3003 (n=9). GLA as a %Control, and GLA+UVI as a %Control+UVI. Data as means±s.e.m. Two-way ANOVA (Tukey&Benjamini-Hochberg). **(f)** Blood glucose in NCD (n=21), FFD (n=56) or GLA+fat-free-diet (GLA, n=55) newborns (P0). Data as means±s.e.m. Kruskal-Wallis test (Dunn's). **(g)** Body weight of NCD (n=34), FFD (n=17) or GLA (n=17) newborns. Data as means±s.e.m. One-way ANOVA (Tukey). **(h)** Suckling score piecharts (%) for 33 NCD, 29 FFD, 18 GLA neonates. **(i)** Cardiac mtFAH gene signature expression from NCD (n=6), FFD (n=8) or GLA (n=21) newborns. Data as means±s.e.m. One-way ANOVA (Tukey&Benjamini-Hochberg). **(j)** Kaplan-Meier curve of FFD (n=64), GLA+LA+fat-free diet milk (n=33), GLA+fat-free-diet milk (n=24) mice. Log-Rank test. (P<0.00001). **(k)** $(AOX)_3$-TK-driven luciferase reporter assay in HEK293.T cells. Cells transfected with: empty vector, wild-type RXRα(LBD) (n=3) or mutated RXRα(LBD)-ΔAF2 (n=3) and stimulated with GLA-BSA. Data as means±s.e.m. Two-way ANOVA (Tukey's). Representative experiment (n=3). **(l)** $(AOX)_3$-TK-driven luciferase reporter assay to assess SRC1 coactivator recruitment (HEK293.T cells). Cells transfected with wild-type RXRα(LBD) (n=3) and/or SRC1 coactivator (n=3), and treated with GLA-BSA. Data as means±s.e.m. Two-way ANOVA (Tukey). Representative experiment (n=3). **(m)** Dose-response curves of GLA-BSA in $(AOX)_3$-TK-driven luciferase assay. HEK293.T cells were transfected with wild-type RXRα(LBD) (n=3). Representative experiment (n=3). Data as means±s.e.m. Non-linear regression. Exact *P* values in Source Data.

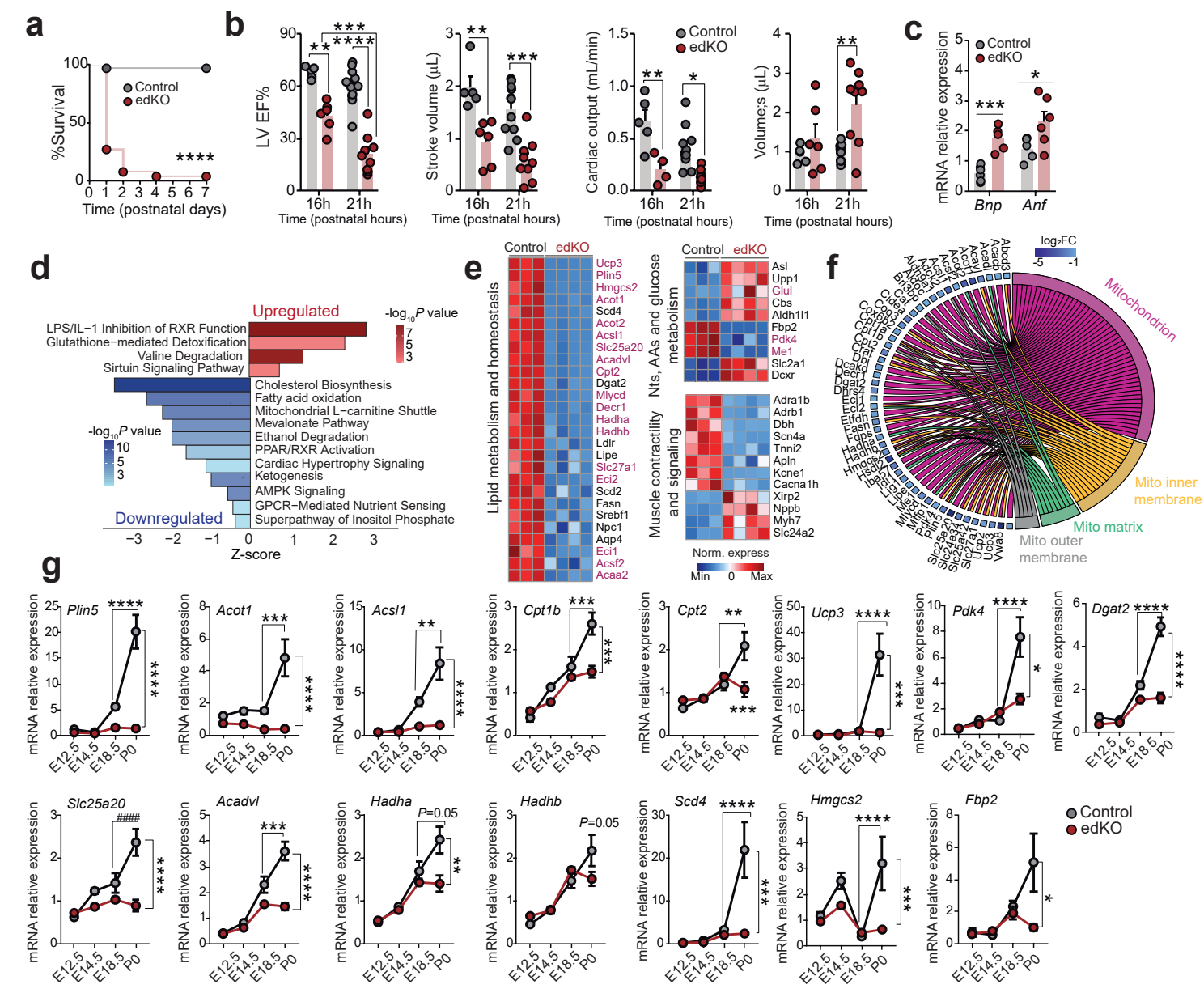
a
%Survival
Control
edKO
Time (postnatal days)
b
LV EF%
Stroke volume (µL)
Cardiac output (mL/min)
Volume;s (µL)
16h
21h
Time (postnatal hours)
c
mRNA relative expression
Bnp
Anf
d
Upregulated
LPS/IL−1 Inhibition of RXR Function
Glutathione−mediated Detoxification
Valine Degradation
Sirtuin Signaling Pathway
Downregulated
Cholesterol Biosynthesis
Fatty acid oxidation
Mitochondrial L−carnitine Shuttle
Mevalonate Pathway
Ethanol Degradation
PPAR/RXR Activation
Cardiac Hypertrophy Signaling
Ketogenesis
AMPK Signaling
GPCR−Mediated Nutrient Sensing
Superpathway of Inositol Phosphate
-log10P value
Z-score
e
Lipid metabolism and homeostasis
Ucp3
Plin5
Hmgcs2
Acot1
Scd4
Acot2
Acsl1
Slc25a20
Acadvl
Cpt2
Dgat2
Mlycd
Decr1
Hadha
Hadhb
Ldlr
Lipe
Slc27a1
Eci2
Scd2
Fasn
Srebf1
Npc1
Aqp4
Eci1
Acsf2
Acaa2
Nts, AAs and glucose metabolism
Asl
Upp1
Glul
Cbs
Aldh1l1
Fbp2
Pdk4
Me1
Slc2a1
Dcxr
Muscle contractility and signaling
Adra1b
Adrb1
Dbh
Scn4a
Tnni2
Apln
Kcne1
Cacna1h
Xirp2
Nppb
Myh7
Slc24a2
Norm. express
Min
0
Max
f
log2FC
Mitochondrion
Mito inner membrane
Mito matrix
Mito outer membrane
g
Plin5
Acot1
Acsl1
Cpt1b
Cpt2
Ucp3
Pdk4
Dgat2
Slc25a20
Acadvl
Hadha
Hadhb
Scd4
Hmgcs2
Fbp2
P=0.05
mRNA relative expression
E12.5
E14.5
E18.5
P0
Control
edKO

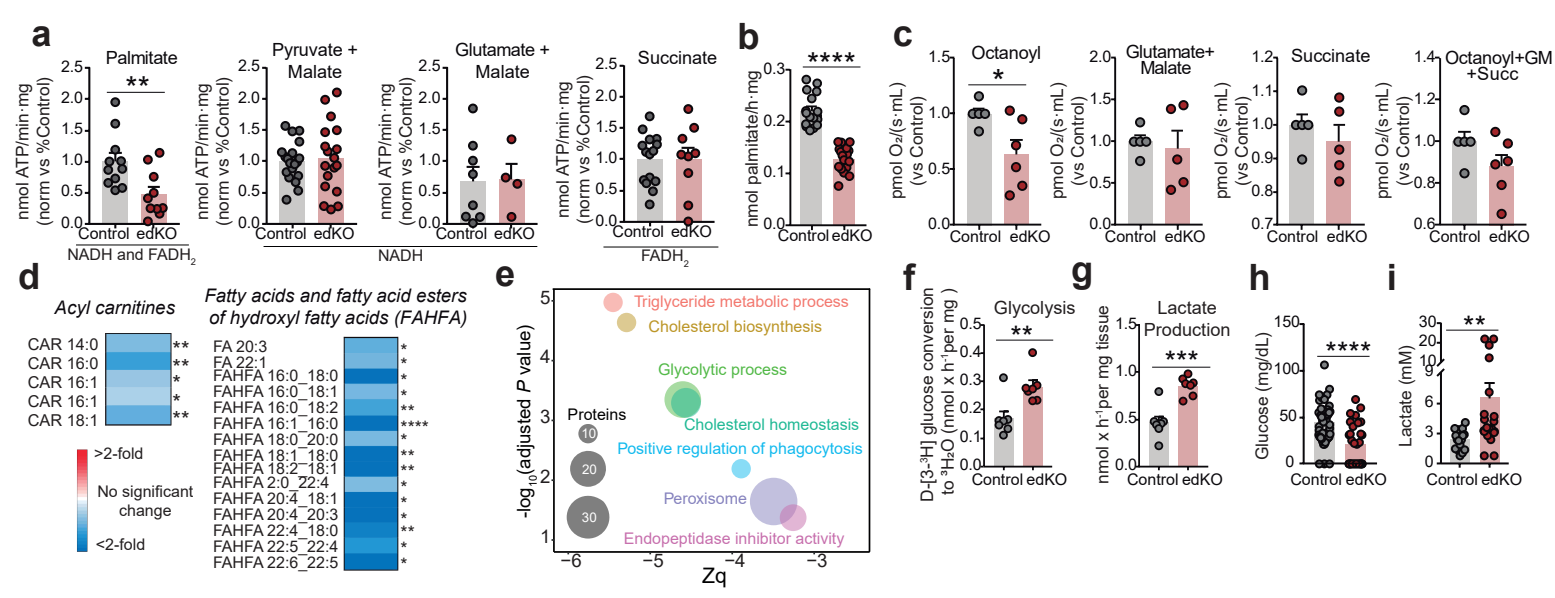
a
Palmitate
Pyruvate + Malate
Glutamate + Malate
Succinate
nmol ATP/min·mg (norm vs %Control)
Control
edKO
NADH and FADH2
NADH
FADH2
b
nmol palmitate/h·mg
****
c
Octanoyl
Glutamate+ Malate
Succinate
Octanoyl+GM +Succ
pmol O2/(s·mL) (vs Control)
d
Acyl carnitines
CAR 14:0
CAR 16:0
CAR 16:1
CAR 16:1
CAR 18:1
>2-fold
No significant change
<2-fold
Fatty acids and fatty acid esters of hydroxyl fatty acids (FAHFA)
FA 20:3
FA 22:1
FAHFA 16:0_18:0
FAHFA 16:0_18:1
FAHFA 16:0_18:2
FAHFA 16:1_16:0
FAHFA 18:0_20:0
FAHFA 18:1_18:0
FAHFA 18:2_18:1
FAHFA 2:0_22:4
FAHFA 20:4_18:1
FAHFA 20:4_20:3
FAHFA 22:4_18:0
FAHFA 22:5_22:4
FAHFA 22:6_22:5
e
Triglyceride metabolic process
Cholesterol biosynthesis
Glycolytic process
Proteins
Cholesterol homeostasis
Positive regulation of phagocytosis
Peroxisome
Endopeptidase inhibitor activity
-log10(adjusted P value)
Zq
f
Glycolysis
D-[3-3H] glucose conversion to 3H2O (nmol x h-1per mg)
g
Lactate Production
nmol x h-1per mg tissue
h
Glucose (mg/dL)
i
Lactate (mM)

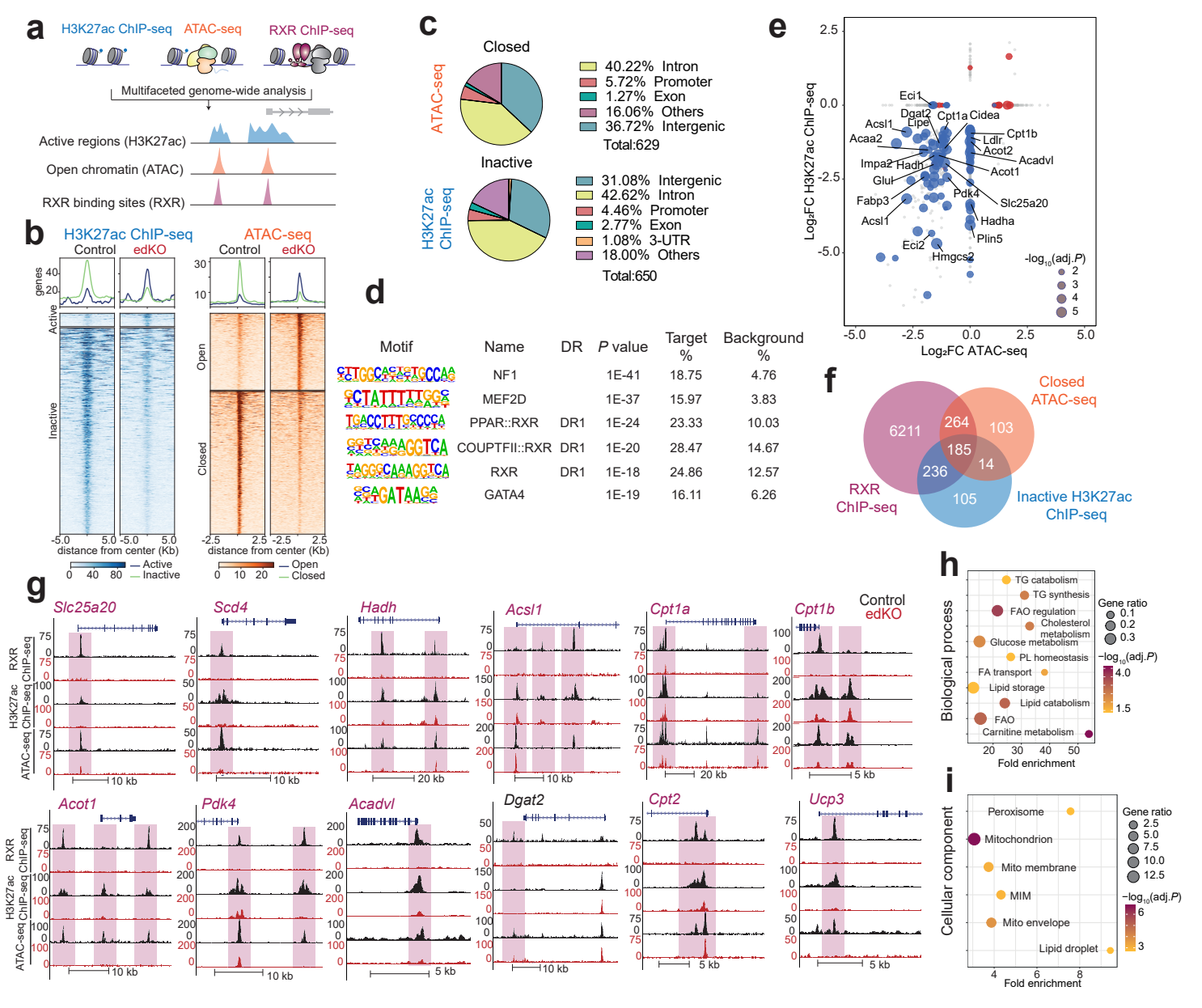
a
H3K27ac ChIP-seq
ATAC-seq
RXR ChIP-seq
Multifaceted genome-wide analysis
Active regions (H3K27ac)
Open chromatin (ATAC)
RXR binding sites (RXR)
b
H3K27ac ChIP-seq
ATAC-seq
Control
edKO
genes
Active
Inactive
Open
Closed
distance from center (Kb)
c
Closed
ATAC-seq
40.22% Intron
5.72% Promoter
1.27% Exon
16.06% Others
36.72% Intergenic
Total:629
Inactive
H3K27ac ChIP-seq
31.08% Intergenic
42.62% Intron
4.46% Promoter
2.77% Exon
1.08% 3-UTR
18.00% Others
Total:650
d
Motif
Name
DR
P value
Target %
Background %
NF1
1E-41
18.75
4.76
MEF2D
1E-37
15.97
3.83
PPAR::RXR
DR1
1E-24
23.33
10.03
COUPTFII::RXR
DR1
1E-20
28.47
14.67
RXR
DR1
1E-18
24.86
12.57
GATA4
1E-19
16.11
6.26
e
Log2FC H3K27ac ChIP-seq
Log2FC ATAC-seq
Eci1
Dgat2
Cpt1a
Cidea
Acsl1
Lipe
Cpt1b
Acaa2
Ldlr
Acot2
Acadvl
Impa2
Hadh
Acot1
Glul
Pdk4
Fabp3
Slc25a20
Acsl1
Hadha
Plin5
Eci2
Hmgcs2
-log10(adj.P)
f
Closed ATAC-seq
Inactive H3K27ac ChIP-seq
RXR ChIP-seq
6211
264
103
185
14
236
105
g
Slc25a20
Scd4
Hadh
Acsl1
Cpt1a
Cpt1b
Control
edKO
RXR ChIP-seq
H3K27ac ChIP-seq
ATAC-seq
Acot1
Pdk4
Acadvl
Dgat2
Cpt2
Ucp3
h
Biological process
TG catabolism
TG synthesis
FAO regulation
Cholesterol metabolism
Glucose metabolism
PL homeostasis
FA transport
Lipid storage
Lipid catabolism
FAO
Carnitine metabolism
Gene ratio
-log10(adj.P)
Fold enrichment
i
Cellular component
Peroxisome
Mitochondrion
Mito membrane
MIM
Mito envelope
Lipid droplet
Gene ratio
-log10(adj.P)
Fold enrichment

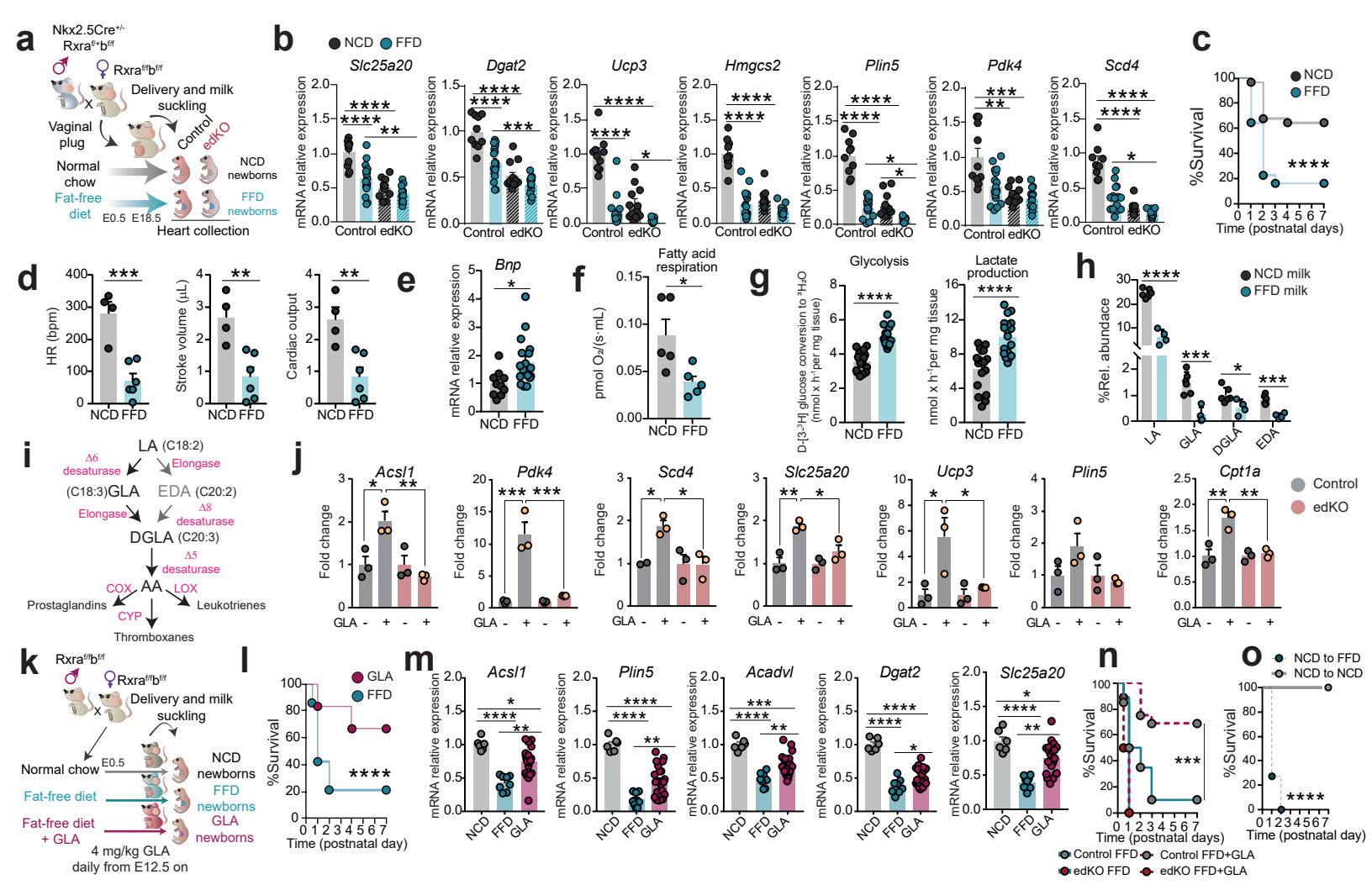
a
Nkx2.5Cre+/-
Rxraf/+bf/f
♂
♀ Rxraf/fbf/f
Delivery and milk suckling
Vaginal plug
Control
edKO
Normal chow
NCD newborns
Fat-free diet
FFD newborns
E0.5 E18.5
Heart collection
b
NCD FFD
Slc25a20
Dgat2
Ucp3
Hmgcs2
Plin5
Pdk4
Scd4
mRNA relative expression
Control edKO
c
NCD
FFD
%Survival
Time (postnatal days)
d
HR (bpm)
Stroke volume (µL)
Cardiac output
NCD FFD
e
Bnp
mRNA relative expression
f
Fatty acid respiration
pmol O2/(s·mL)
g
Glycolysis
Lactate production
D-[3-3H] glucose conversion to 3H2O (nmol x h-1 per mg tissue)
nmol x h-1 per mg tissue
h
NCD milk
FFD milk
%Rel. abundace
LA
GLA
DGLA
EDA
i
LA (C18:2)
Δ6 desaturase
Elongase
(C18:3)GLA
EDA (C20:2)
Δ8 desaturase
DGLA (C20:3)
Δ5 desaturase
COX
LOX
AA
Prostaglandins
Leukotrienes
CYP
Thromboxanes
j
Acsl1
Pdk4
Scd4
Slc25a20
Ucp3
Plin5
Cpt1a
Fold change
GLA
Control
edKO
k
Rxraf/fbf/f
♂
♀ Rxraf/fbf/f
Delivery and milk suckling
Normal chow
E0.5
NCD newborns
Fat-free diet
FFD newborns
Fat-free diet + GLA
GLA newborns
4 mg/kg GLA daily from E12.5 on
l
GLA
FFD
%Survival
Time (postnatal day)
m
Acsl1
Plin5
Acadvl
Dgat2
Slc25a20
mRNA relative expression
NCD FFD GLA
n
%Survival
Time (postnatal days)
Control FFD
Control FFD+GLA
edKO FFD
edKO FFD+GLA
o
NCD to FFD
NCD to NCD
%Survival
Time (postnatal day)

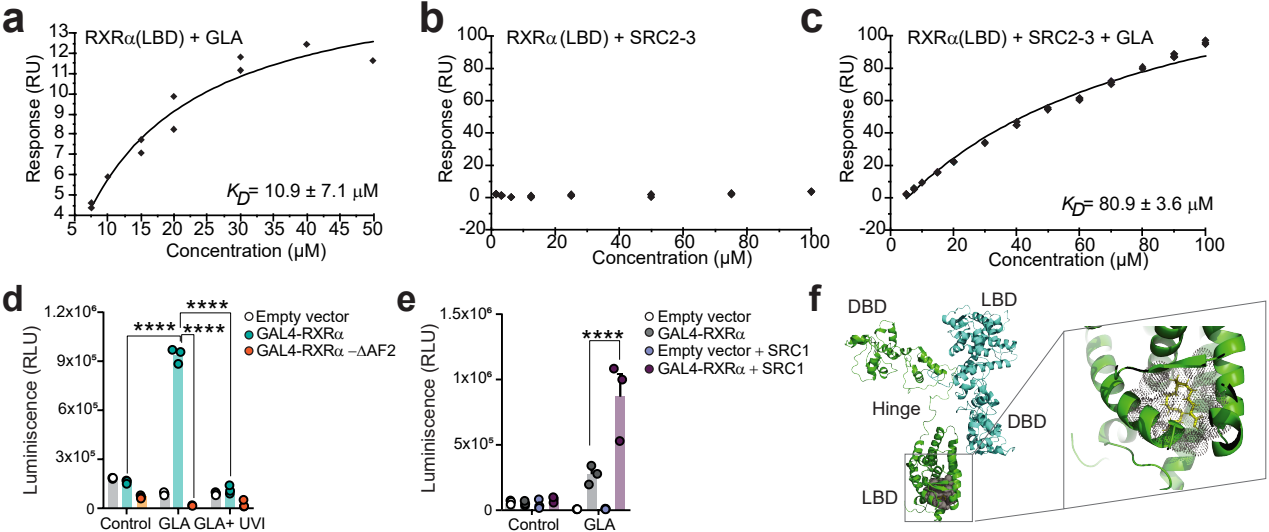
a
RXRα(LBD) + GLA
Response (RU)
Concentration (μM)
K_D= 10.9 ± 7.1 μM
b
RXRα (LBD) + SRC2-3
Response (RU)
Concentration (μM)
c
RXRα(LBD) + SRC2-3 + GLA
Response (RU)
Concentration (μM)
K_D= 80.9 ± 3.6 μM
d
Luminiscence (RLU)
Empty vector
GAL4-RXRα
GAL4-RXRα −ΔAF2
****
Control
GLA
GLA+ UVI
e
Luminiscence (RLU)
Empty vector
GAL4-RXRα
Empty vector + SRC1
GAL4-RXRα + SRC1
****
Control
GLA
f
DBD
LBD
Hinge
DBD
LBD

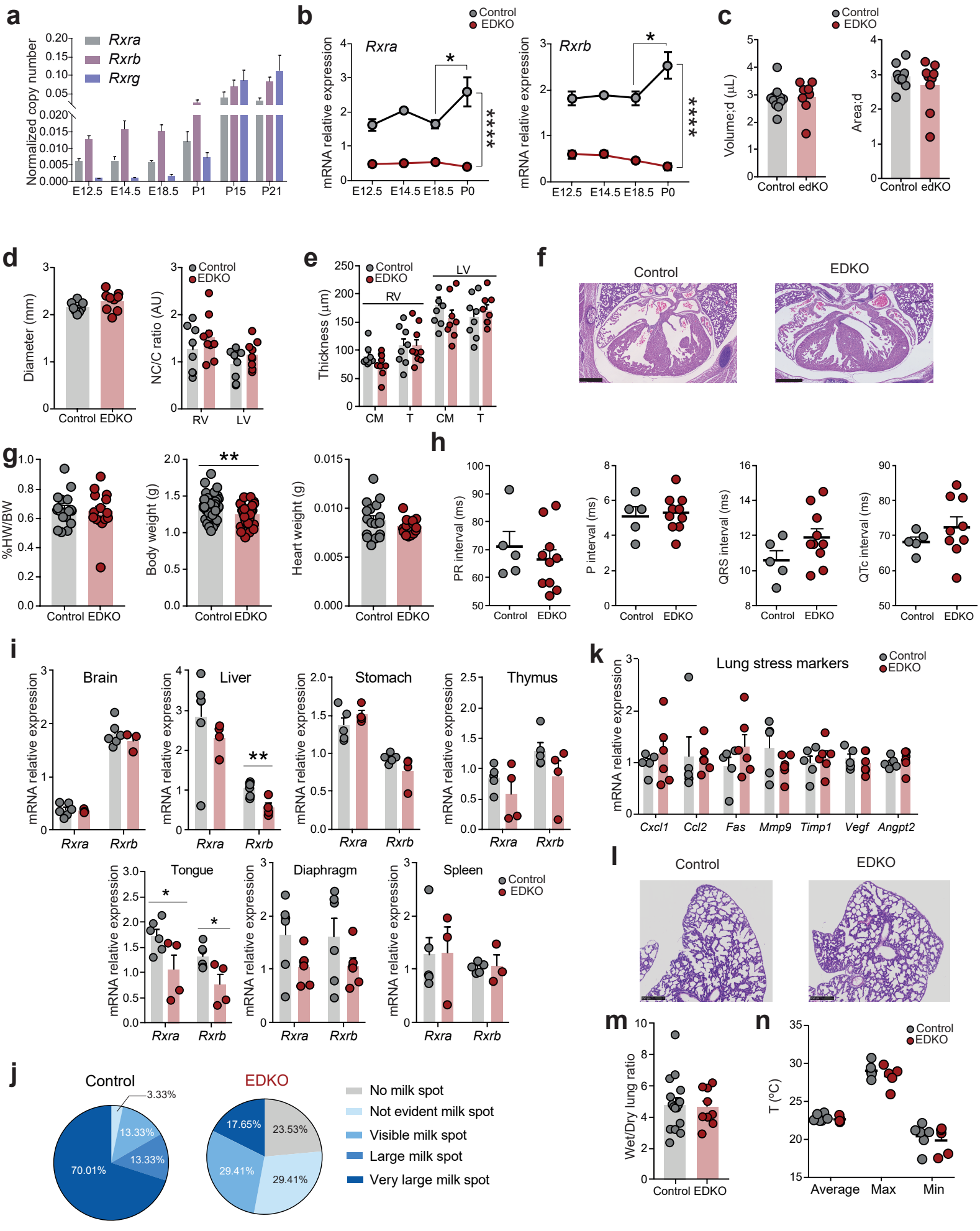
a
Normalized copy number
Rxra
Rxrb
Rxrg
E12.5 E14.5 E18.5 P1 P15 P21
b
Control
EDKO
Rxra
Rxrb
mRNA relative expression
E12.5 E14.5 E18.5 P0
****
c
Volume;d (µL)
Area;d
Control edKO
d
Diameter (mm)
NC/C ratio (AU)
RV LV
e
Thickness (µm)
RV
LV
CM T CM T
f
Control
EDKO
g
%HW/BW
Body weight (g)
Heart weight (g)
h
PR interval (ms)
P interval (ms)
QRS interval (ms)
QTc interval (ms)
i
Brain
Liver
Stomach
Thymus
Tongue
Diaphragm
Spleen
Rxra Rxrb
k
Lung stress markers
Cxcl1 Ccl2 Fas Mmp9 Timp1 Vegf Angpt2
l
m
Wet/Dry lung ratio
n
T (°C)
Average Max Min
j
Control
EDKO
3.33%
13.33%
13.33%
70.01%
17.65%
23.53%
29.41%
29.41%
No milk spot
Not evident milk spot
Visible milk spot
Large milk spot
Very large milk spot

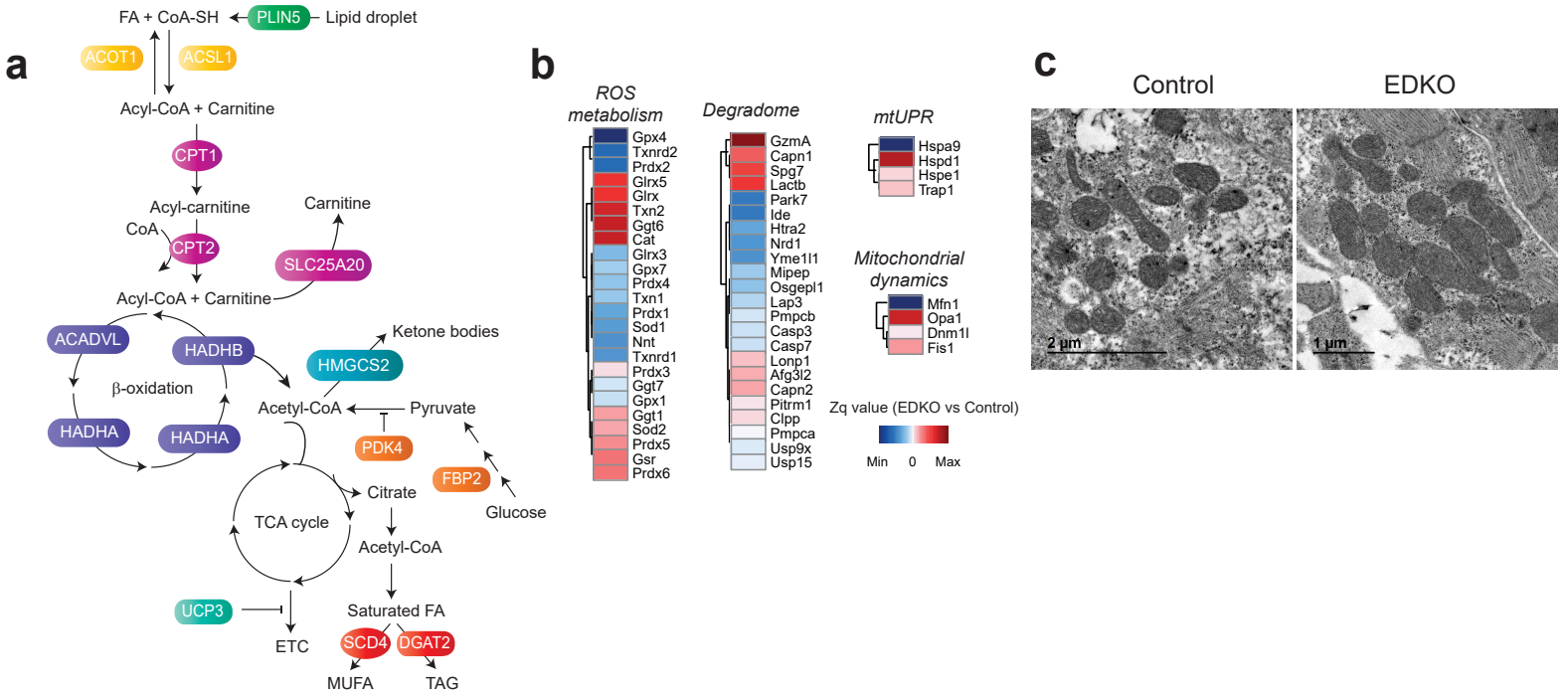
a
FA + CoA-SH
PLIN5
Lipid droplet
ACOT1
ACSL1
Acyl-CoA + Carnitine
CPT1
Acyl-carnitine
CoA
CPT2
Carnitine
SLC25A20
Acyl-CoA + Carnitine
ACADVL
HADHB
Ketone bodies
HMGCS2
β-oxidation
Acetyl-CoA
Pyruvate
HADHA
HADHA
PDK4
FBP2
Glucose
Citrate
TCA cycle
Acetyl-CoA
UCP3
Saturated FA
ETC
SCD4
DGAT2
MUFA
TAG
b
ROS metabolism
Gpx4
Txnrd2
Prdx2
Glrx5
Glrx
Txn2
Ggt6
Cat
Glrx3
Gpx7
Prdx4
Txn1
Prdx1
Sod1
Nnt
Txnrd1
Prdx3
Ggt7
Gpx1
Ggt1
Sod2
Prdx5
Gsr
Prdx6
Degradome
GzmA
Capn1
Spg7
Lactb
Park7
Ide
Htra2
Nrd1
Yme1l1
Mipep
Osgepl1
Lap3
Pmpcb
Casp3
Casp7
Lonp1
Afg3l2
Capn2
Pitrm1
Clpp
Pmpca
Usp9x
Usp15
mtUPR
Hspa9
Hspd1
Hspe1
Trap1
Mitochondrial dynamics
Mfn1
Opa1
Dnm1l
Fis1
Zq value (EDKO vs Control)
Min
0
Max
c
Control
EDKO
2 µm
1 µm

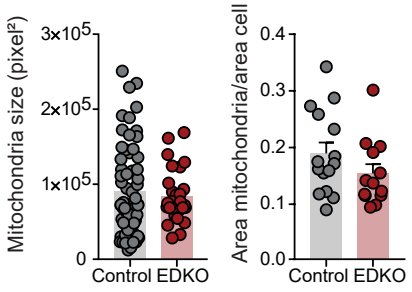
d
Mitochondria size (pixel²)
3x10⁵
2x10⁵
1x10⁵
0
Control EDKO
Area mitochondria/area cell
0.4
0.3
0.2
0.1
0.0
Control EDKO

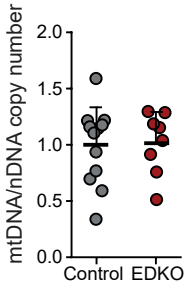
e
mtDNA/nDNA copy number
2.0
1.5
1.0
0.5
0.0
Control EDKO

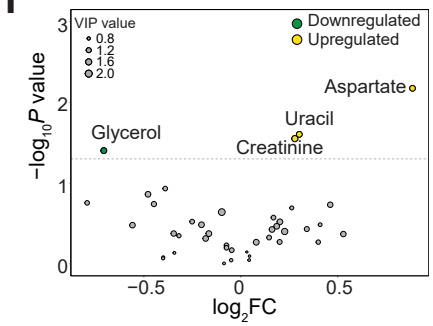
f
VIP value
0.8
1.2
1.6
2.0
Downregulated
Upregulated
Aspartate
Uracil
Glycerol
Creatinine
−log10P value
3
2
1
0
−0.5
0
0.5
log2FC

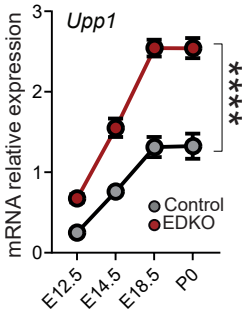
g
Upp1
mRNA relative expression
3
2
1
0
****
Control
EDKO
E12.5
E14.5
E18.5
P0

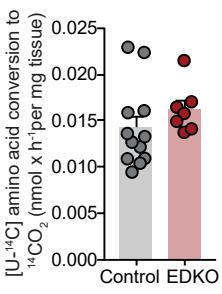
h
[U-14C] amino acid conversion to 14CO2 (nmol x h-1per mg tissue)
0.025
0.020
0.015
0.010
0.005
0.000
Control EDKO

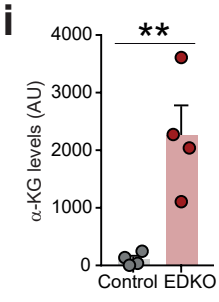
i
α-KG levels (AU)
4000
3000
2000
1000
0
**
Control EDKO

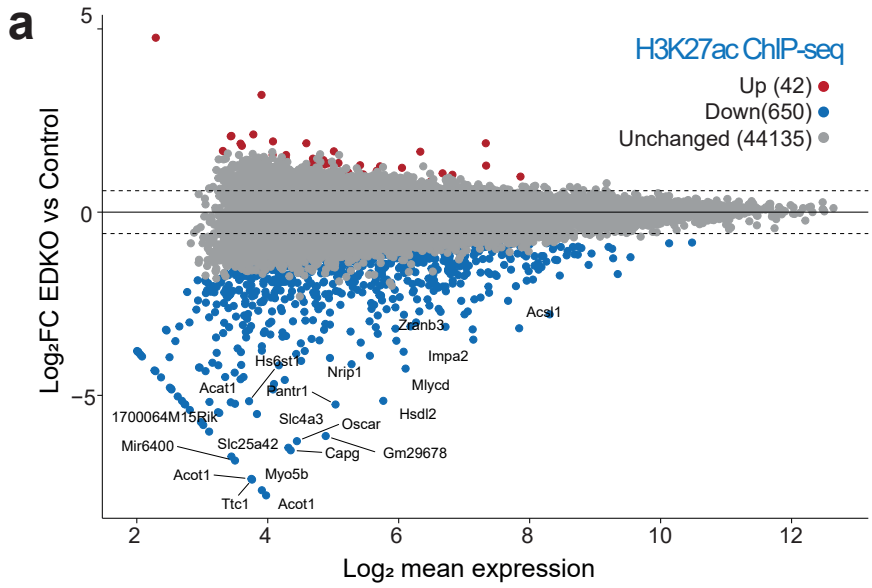

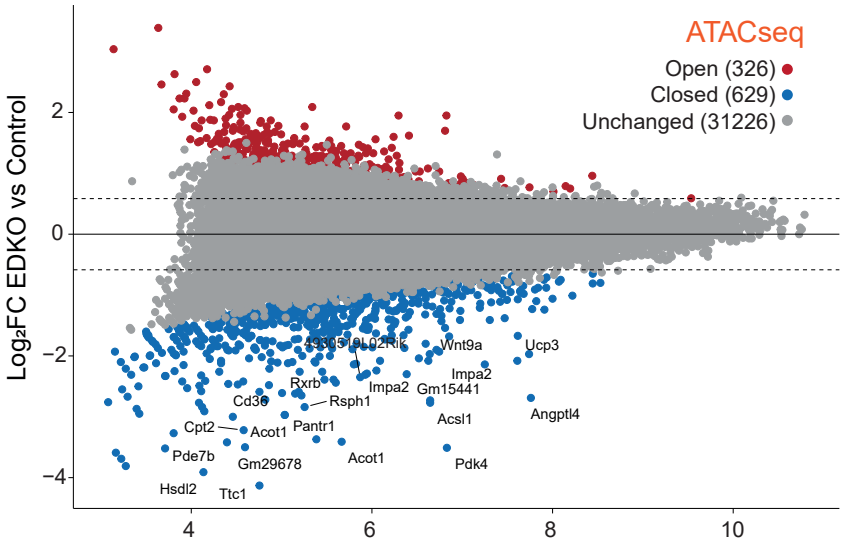

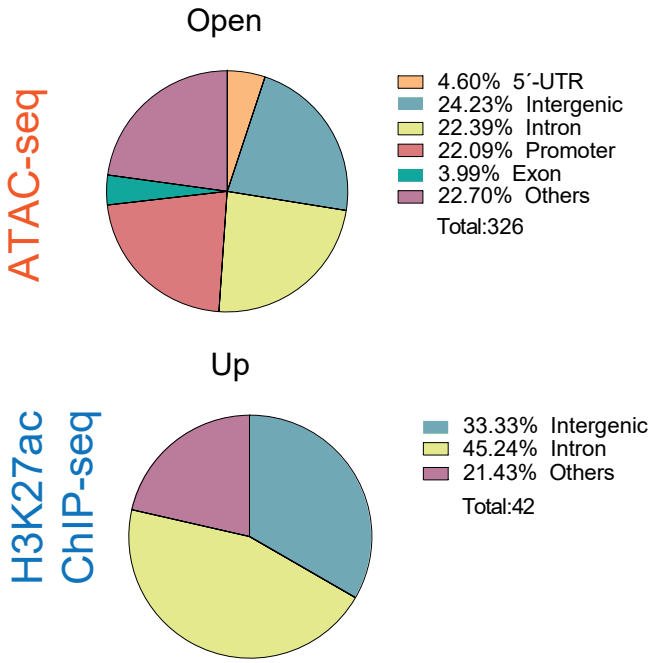

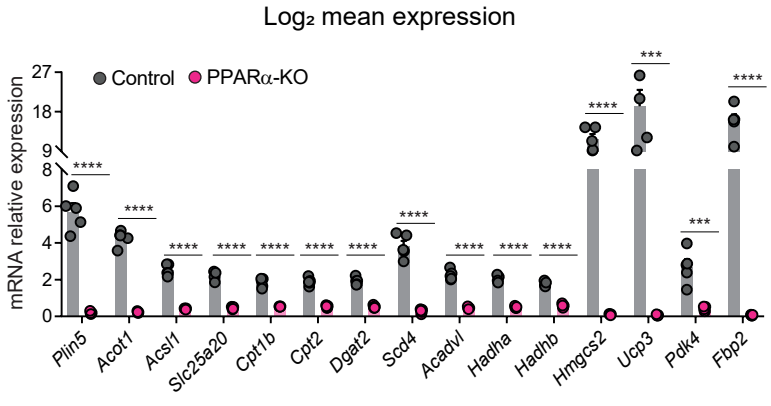

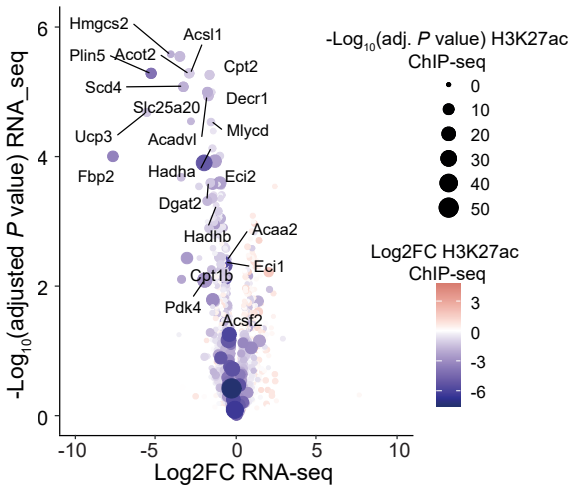

e

Motif	Name	DR	*P* value	Target %	Background %
	RXR::THR	DR4	1E-884	16.43	4.22
	RXR::COUPTFII	half-site	1E-770	34.38	16.41
	RXR::COUPTFIII	DR1	1E-766	28.83	12.44
	RXR::RAR	half-site	1E-570	41.26	24.18
	ERRA	half-site	1E-392	35.88	22.18
	MEF2B		1E-329	10.15	3.67
	RXR::PPAR	DR1	1E-270	18.11	9.67
	RXR	DR1	1E-204	19.62	11.80
	GATA4		1E-172	10.32	5.18

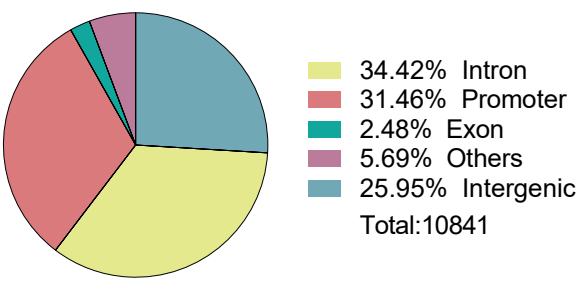

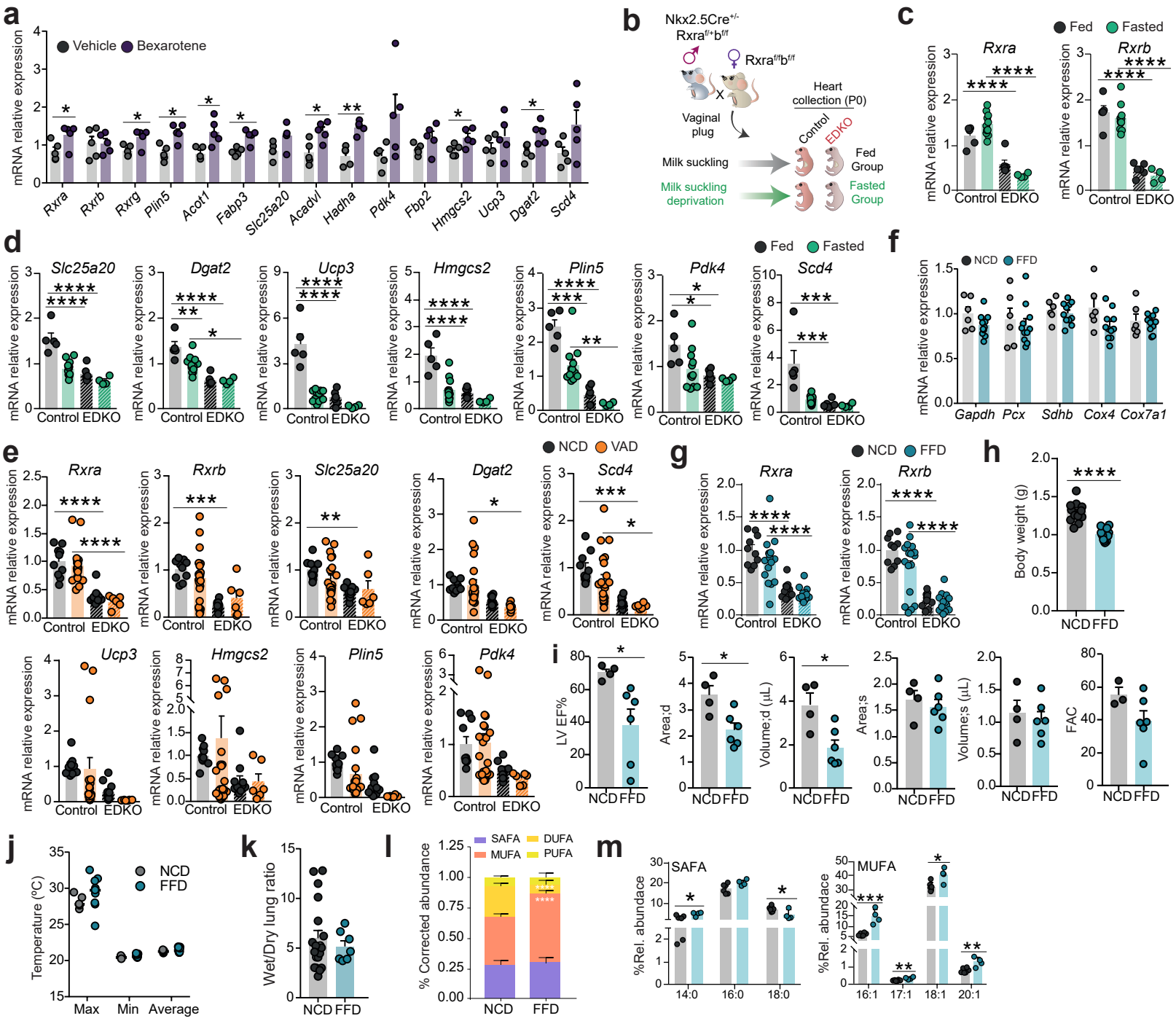
a
Vehicle
Bexarotene
mRNA relative expression
Rxra
Rxrb
Rxrg
Plin5
Acot1
Fabp3
Slc25a20
Acadvl
Hadha
Pdk4
Fbp2
Hmgcs2
Ucp3
Dgat2
Scd4
b
Nkx2.5Cre+/-
Rxraf/+bf/f
Rxraf/fbf/f
Vaginal plug
Heart collection (P0)
Control
EDKO
Milk suckling
Fed Group
Milk suckling deprivation
Fasted Group
c
Fed
Fasted
Rxra
Rxrb
Control EDKO
d
Slc25a20
Dgat2
Ucp3
Hmgcs2
Plin5
Pdk4
Scd4
e
NCD
VAD
f
NCD
FFD
Gapdh
Pcx
Sdhb
Cox4
Cox7a1
g
h
Body weight (g)
i
LV EF%
Area;d
Volume;d (µL)
Area;s
Volume;s (µL)
FAC
j
Temperature (ºC)
Max
Min
Average
k
Wet/Dry lung ratio
l
% Corrected abundance
SAFA
MUFA
DUFA
PUFA
m
%Rel. abundace
14:0
16:0
18:0
16:1
17:1
18:1
20:1

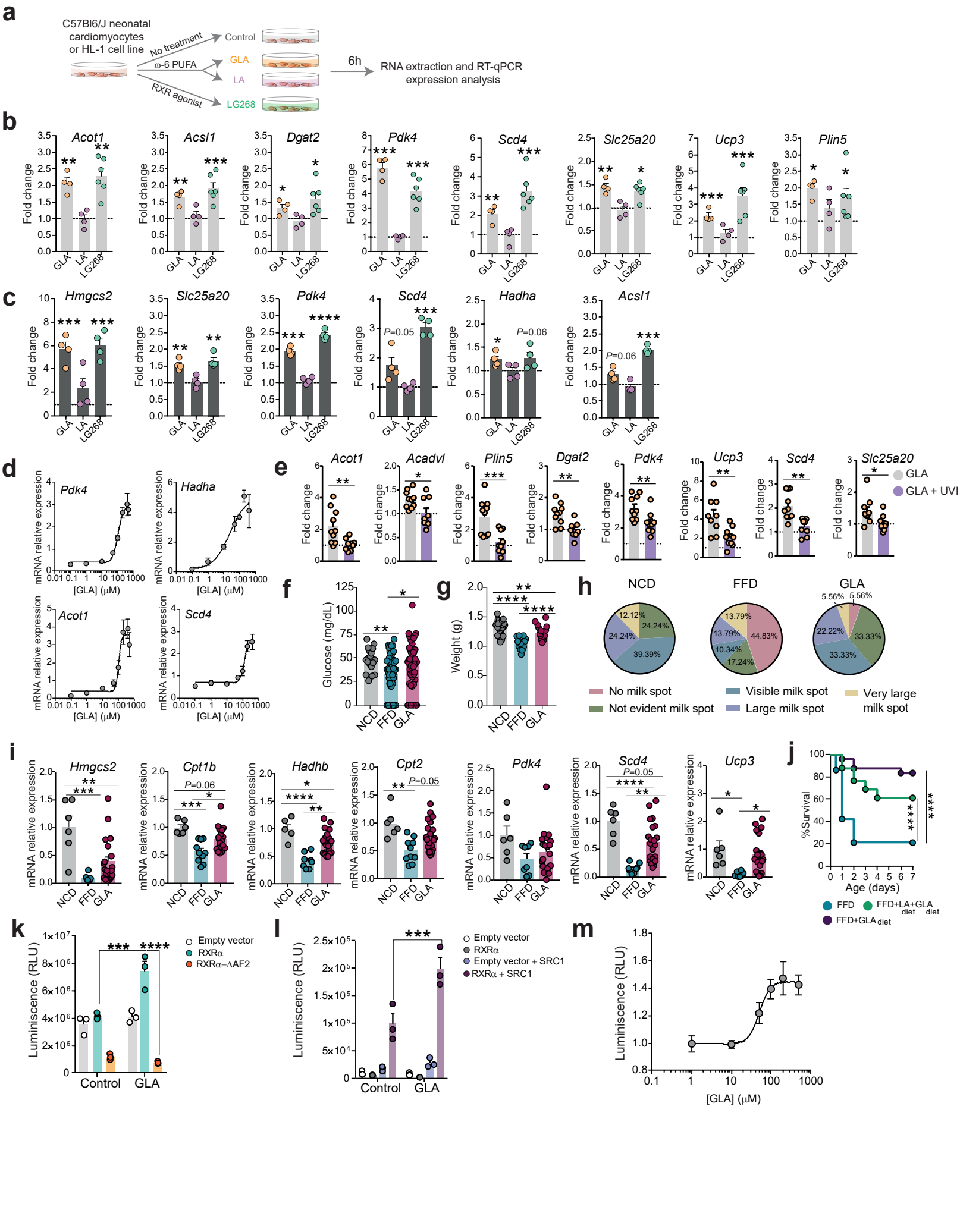
a
C57Bl6/J neonatal cardiomyocytes or HL-1 cell line
No treatment
Control
ω-6 PUFA
GLA
LA
RXR agonist
LG268
6h
RNA extraction and RT-qPCR expression analysis
b
Acot1
Acsl1
Dgat2
Pdk4
Scd4
Slc25a20
Ucp3
Plin5
Fold change
GLA
LA
LG268
c
Hmgcs2
Slc25a20
Pdk4
Scd4
Hadha
Acsl1
P=0.05
P=0.06
d
Pdk4
Hadha
Acot1
Scd4
mRNA relative expression
[GLA] (μM)
e
Acot1
Acadvl
Plin5
Dgat2
Pdk4
Ucp3
Scd4
Slc25a20
GLA
GLA + UVI
f
Glucose (mg/dL)
NCD
FFD
GLA
g
Weight (g)
h
NCD
FFD
GLA
12.12%
24.24%
24.24%
39.39%
13.79%
44.83%
13.79%
10.34%
17.24%
5.56%
5.56%
22.22%
33.33%
33.33%
No milk spot
Not evident milk spot
Visible milk spot
Large milk spot
Very large milk spot
i
Hmgcs2
Cpt1b
Hadhb
Cpt2
Pdk4
Scd4
Ucp3
mRNA relative expression
j
%Survival
Age (days)
FFD
FFD+LA+GLA diet
FFD+GLA diet
k
Luminiscence (RLU)
Empty vector
RXRα
RXRα–ΔAF2
Control
GLA
l
Empty vector
RXRα
Empty vector + SRC1
RXRα + SRC1
m
Luminiscence (RLU)
[GLA] (μM)